affinity of HbV (P_{50} = 30) is close to that of the hamster RBC (P_{50} = 28), the Hill number of HbV is smaller than that of RBC. Comparing the slopes of the curves at around P_{50}, RBC is steeper than HbV (P_{50} = 30). Conversely, in the range of 60–50 mmHg, which corresponds to O_2 tensions at the aorta (Pa_{O_2}) and the entrance of the microvasculature (A_1), HbV (P_{50} = 30) is steeper than the hamster RBC. This indicates that HbV (P_{50} = 30) releases a larger amount of O_2 in large arteries than RBC does, which may induce autoregulatory response to overabundant O_2 and resulting in constriction of upstream arteries, which are larger than A_1. HbV (P_{50} = 16), which shows a gentler slope, may induce less vasoconstriction. In the case of HbV (P_{50} = 9), the absolute amount of unloaded O_2 may be crucial. Considering this hypothesis, the better slope of HbV at around 50 mmHg should be identical to that of RBC, and at this condition P_{50} should be 22 mmHg because the Hill number of HbV is smaller than that of RBC. However, it is impossible to regulate both the O_2 affinity and O_2-releasing rate to be identical to those of RBC, which is a limitation due to the small size of HbV.

Other mechanisms may also contribute to the reduction in blood flow relative to baseline, such as influences of the complement activation and active oxygen production, which may alter the microvascular perfusion.

In conclusion, the present experiments with three kinds of HbVs with different P_{50} and same other physical properties show that microvascular perfusion and O_2 tensions of the three HbV-HSA groups were much improved in comparison with the HSA group; these parameters were slightly improved by decreasing P_{50} from 30 to 16 mmHg, which appears to be an optimal value for P_{50} in this system. Further increasing P_{50} to 9 mmHg reversed the trend, indicating that facilitated O_2 unloading of HbV by decreasing the O_2 affinity with PLP as an allosteric effector is important. This result indicates that the optimal O_2 dissociation curve of HbV in the normoxic condition, from the view point of microvascular perfusion, may be left shifted relative to blood.

The authors gratefully acknowledge Dr. Robert M. Winslow for supervising the study of blood substitutes. The authors also thank Dr. K. D. Vandegriff for the discussion on the stopped flow analysis, Dr. M. McCarthy for the oncotic pressure and O_2 capacity measurements, and Dr. S. I. Park and T. Kose, M. Aburatani, and K. Hamazaki for the HbV preparation.

This work has been supported in part by National Heart, Lung, and Blood Institute Program Project HL-48018 and Grants-in-Aid for Scientific Research from the Ministry of Education, Science, Sports and Culture, Japan (Grant 07508005). H. Sakai was an overseas research fellow of the Japan Society for the Promotion of Science.

Addresses for reprint requests and correspondence: M. Intaglietta, Dept. of Bioengineering, University of California, San Diego, 9500 Gilman Dr., La Jolla, CA 92093-0412; E. Tsuchida, Dept. of Polymer Chemistry, Advanced Research Institute for Science and Engineering, Waseda Univ., Tokyo 169-8555, Japan.

Received 17 February 1998; accepted in final form 13 October 1998.

REFERENCES

1. **Conover, C. D., P. Malatesta, L. Lejeune, C. L. Chang, and R. G. L. Shorr.** The effect of hemodilution with polyethylene glycol bovine hemoglobin (PEG-Hb) in a conscious porcine model. *J. Investig. Med.* 44: 238–246, 1996.
2. **Detar, R., and D. F. Bohr.** Oxygen and vascular smooth muscle contraction. *Am. J. Physiol.* 214: 241–244, 1968.
3. **Djordjevich, L., J. Mayoral, I. F. Miller, and A. D. Ivankovich.** Cardiorespiratory effects of exchange transfusions with synthetic erythrocytes in rats. *Crit. Care Med.* 15: 318–323, 1987.
4. **Ellsworth, M. L., and R. N. Pittman.** Arterioles supply oxygen to capillaries by diffusion as well as convection. *Am. J. Physiol.* 258 (*Heart Circ. Physiol.* 27): H1240–H1243, 1990.
6. **Gutierrez, G., and J. M. Andry.** Increased hemoglobin O_2 affinity does not improve O_2 consumption in hypoxemia. *J. Appl. Physiol.* 66: 837–843, 1989.
7. **Harder, D. R., J. Narayaran, E. K. Birks, J. Francois Liard, J. D. Imig, J. H. Lombard, A. R. Lange, and R. J. Roman.** Identification of a putative microvascular oxygen sensor. *Circ. Res.* 79: 54–61, 1996.
8. **Intaglietta, M.** Whitaker lecture 1996: microcirculation, biomedical engineering and artificial blood. *Ann. Biomed. Eng.* 25: 593–603, 1997.
9. **Intaglietta, M., P. C. Johnson, and R. M. Winslow.** Microvascular and tissue oxygen distribution. *Cardiovasc. Res.* 32: 632–643, 1996.
10. **Johnson, P. C.** Autoregulation of blood flow. *Circ. Res.* 59: 483–495, 1986.
11. **Keipert, P. E., A. Gonzales, G. L. Gomez, V. W. Macdonald, J. R. Hess, and R. M. Winslow.** Acute changes in systemic blood pressure and urine output of conscious rats following exchange transfusion with diaspirin-crosslinked hemoglobin solution. *Transfusion* 33: 701–708, 1993.
12. **Kerger, H., D. J. Saltzman, A. Gonzales, A. G. Tsai, K. van Ackern, R. M. Winslow, and M. Intaglietta.** Microvascular oxygen delivery and interstitial oxygenation during sodium pentobarbital anesthesia. *Anesthesiology* 86: 372–386, 1997.
13. **Kerger, H., I. P. Torres Filho, M. Rivas, R. M. Winslow, and M. Intaglietta.** Systemic and subcutaneous microvascular oxygen tension in conscious Syrian golden hamsters. *Am. J. Physiol.* 268 (*Heart Circ. Physiol.* 37): H802–H810, 1995.
14. **Koehler, R. C., R. J. Traystman, and M. D. Johnes, Jr.** Regional blood flow and O_2 transport during hypoxic and CO hypoxia in neonatal and adult sheep. *Am. J. Physiol.* 248 (*Heart Circ. Physiol.* 17): H118–H124, 1985.
15. **Liard, J. F, and M. P. Kunert.** Hemodynamic changes induced by low blood oxygen affinity in dogs. *Am. J. Physiol.* 264 (*Regulatory Integrative Comp. Physiol.* 33): R396–R401, 1993.
16. **Messina, E. J., D. Sun, A. Koller, M. S. Wolin, and G. Kaley.** Increase in oxygen tension evoke arteriolar constriction by inhibiting endothelial prostaglandin synthesis. *Microvasc. Res.* 48: 151–160, 1994.
17. **Mirhashemi, S., G. A. Breit, R. H. Chavez Chavez, and M. Intaglietta.** Effects of hemodilution on skin microcirculation. *Am. J. Physiol.* 254 (*Heart Circ. Physiol.* 23): H411–H416, 1988.
18. **Moncada, S., R. M. J. Palmer, and E. A. Higgs.** Nitric oxide: physiology, pathophysiology, and pharmacology. *Pharmacol. Rev.* 43: 109–142, 1991.
19. **Nakai, K., T. Ohta, I. Sakuma, K. Akama, Y. Kobayashi, S. Tokuyama, A. Kitabatake, Y. Nakazato, T. A. Takahashi, and S. Sekiguchi.** Inhibition of endothelium-dependent relaxation by hemoglobin in rabbit aortic strips: comparison between acellular hemoglobin derivatives and cellular hemoglobins. *J. Cardiovasc. Pharmacol.* 28: 115–123, 1996.
20. **Rudolph, A. S.** Encapsulation of hemoglobin in liposomes. In: *Blood Substitutes: Physiological Basis of Efficacy*, edited by R. M. Winslow, K. D. Vandegriff, and M. Intaglietta. Boston, MA: Birkhäuser, 1995, p. 90–104.
21. **Sakai, H., K. Hamada, S. Takeoka, H. Nishide, and E. Tsuchida.** Physical characteristics of hemoglobin vesicles as red cell substitutes. *Biotechnol. Progress* 12: 119–125, 1996.
22. **Sakai, H., H. Hara, A. G. Tsai, E. Tsuchida, P. C. Johnson, and M. Intaglietta.** Changes in resistance vessels during hemorrhagic shock and resuscitation in conscious hamster model. *Am. J. Physiol.* 276 (*Heart Circ. Physiol.* 45): H563–H571, 1999.
23. **Sakai, H., S. Takeoka, S. I. Park, T. Kose, K. Hamada, Y. Izumi, A. Yoshizu, H. Nishide, K. Kobayashi, and E. Tsu-**

chida. Surface modification of hemoglobin vesicles with poly(ethyleneglycol) and effects on aggregation, viscosity, and blood flow during 90% exchange transfusion in anesthetized rats. *Bioconjug. Chem.* 8: 15–22, 1997.

24. **Sakai, H., A. G. Tsai, H. Kerger, S. I. Park, S. Takeoka, H. Nishide, E. Tsuchida, and M. Intaglietta.** Subcutaneous microvascular responses to hemodilution with red cell substitutes consisting of polyethyleneglycol-modified vesicles encapsulating hemoglobin. *J. Biomed. Mater. Res.* 40: 66–78, 1998.
25. **Schlichtig, R., D. J. Kramer, and M. R. Pinsky.** Flow redistribution during progressive hemorrhage is a determinant of a critical O_2 delivery. *J. Appl. Physiol.* 70: 169–178, 1991.
26. **Schultz, S. C., B. Grady, F. Cole, I. Hamilton, K. Burhop, and D. S. Malcolm.** A role for endothelin and nitric oxide in the pressor response to diaspirin cross-linked hemoglobin. *J. Lab. Clin. Med.* 122: 301–308, 1993.
27. **Schumacker, P. T., A. J. Suggett, P. D. Wagner, and J. B. West.** Role of hemoglobin P_{50} in O_2 transport during normoxic and hypoxic exercise in the dog. *J. Appl. Physiol.* 59: 749–757, 1985.

27a. **Stein, C. J., and M. L. Ellsworth.** Microvascular oxygen transport: impact of a left-shifted dissociation curve. *Am. J. Physiol.* 262 (*Heart Circ. Physiol.* 31): H517–H522, 1992.

28. **Swain, D. P., and R. N. Pittman.** Oxygen exchange in the microcirculation of hamster retractor muscle. *Am. J. Physiol.* 256 (*Heart Circ. Physiol.* 25): H247–H255, 1989.
29. **Teisseire, B., C. Ropars, M.-C. Villereal, and C. Nicolau.** Long-term physiological effects of enhanced O_2 release by inositol hexaphosphate-loaded erythrocytes. *Proc. Natl. Acad. Sci. USA* 84: 6894–6898, 1987.
30. **Turek, Z., F. Kreuzer, M. Turek-Maischeider, and B. E. M. Ringnalda.** Blood O_2 content, cardiac output, and flow to organs at several levels of oxygenation in rats with a left-shifted blood oxygen dissociation curve. *Pflügers Arch.* 376: 201–207, 1978.
31. **Vandegriff, K. D., and J. S. Olson.** Morphological and physiological factors affecting oxygen uptake and release by red blood cell. *J. Biol. Chem.* 259: 12619–12627, 1984.
32. **Vandegriff, K. D., and R. M. Winslow.** A theoretical analysis of oxygen transport: a new strategy for the design of hemoglobin-based red cell substitutes. In: *Blood Substitutes: Physiological Basis of Efficacy*, edited by R. M. Winslow, K. D. Vandegriff, and M. Intaglietta. Boston: Birkhäuser, 1995, p. 143–154.
33. **Wang, L., K. Morizawa, S. Tokuyama, T. Satoh, and E. Tsuchida.** Modulation of oxygen-carrying capacity of artificial red cells (ARC). *Polym. Adv. Technol.* 4: 8–11, 1992.
34. **Winslow, R. M.** Blood substitutes. *Sci. Med. March/April:* 54–63, 1997.
35. **Woodson, R. D., and S. Auerbach.** Effect of increased oxygen affinity and anemia on cardiac output and its distribution. *J. Appl. Physiol.* 53: 1299–1306, 1982.

Changes in resistance vessels during hemorrhagic shock and resuscitation in conscious hamster model

HIROMI SAKAI,[1,2] HIROYUKI HARA,[1,2] AMY G. TSAI,[1] EISHUN TSUCHIDA,[2] PAUL C. JOHNSON,[1] AND MARCOS INTAGLIETTA[1]

[1]*Department of Bioengineering, University of California, San Diego, La Jolla, California, 92093-0412; and* [2]*Department of Polymer Chemistry, Advanced Research Institute for Science and Engineering, Waseda University, Tokyo 169-8555, Japan*

Sakai, Hiromi, Hiroyuki Hara, Amy G. Tsai, Eishun Tsuchida, Paul C. Johnson, and Marcos Intaglietta. Changes in resistance vessels during hemorrhagic shock and resuscitation in conscious hamster model. *Am. J. Physiol.* 276 (*Heart Circ. Physiol.* 45): H563–H571, 1999.—The unanesthetized hamster dorsal skinfold preparation was used to monitor diameters and blood flow rates in resistance arteries (small arteries, A_0: diameter, 156 ± 23 μm) and capacitance vessels (small veins, V_0: 365 ± 64 μm), during 45 min of hemorrhagic shock at 40 mmHg mean arterial pressure (MAP) and resuscitation. A_0 and V_0 vessels constricted significantly to 52 and 70% of the basal values, respectively, whereas precapillary arterioles (A_1–A_4, 8–60 μm) and collecting venules (V_C–V_L, 26–80 μm) did not change or tended to dilate. Blood flow rates in the microvessels declined to <20% of the basal values. Resuscitation with shed autologous blood (SAB) showed incomplete recovery of A_0 and V_0 diameters even 2 h after resuscitation (71 ± 14% and 81 ± 18%, respectively, of basal value), whereas other vessels did not change significantly. The behavior of A_0 diameter coincided with the incomplete recovery of blood flow rates in all the vessels (ca. 50%) according to Poiseuille's law, and the incomplete recovery of functional capillary density (ca. 75%). Resuscitation with 8% human serum albumin in saline (HSA) tended to show higher levels of A_0 constriction and A_4 dilation and lowered blood flow rates. Resuscitation with SAB restored tissue P_{O_2} 27 ± 10 mmHg after 2 h, which was near control levels (28 ± 5 mmHg), whereas resuscitation with HSA caused tissue P_{O_2} to remain significantly depressed (6 ± 2 mmHg), and flow rates were significantly lower than resuscitation with SAB. These results indicate that response of the A_0 vessels is the crucial determinant of blood flow in the observed area. The constriction of A_0 may help sustain MAP, and constriction of V_0 may enhance blood redistribution from the skin to the vital organs under the hypotensive condition.

feeding artery; vasoconstriction; autologous blood; albumin; microcirculation

IT HAS BEEN SHOWN in some vascular beds that approximately one-half of the total blood pressure drop across the microvasculature occurs in small arteries and large arterioles (5, 43). They are sometimes referred to as the "resistance arteries" in vascular networks of tissues such as the mesentery, pia mater, skeletal muscle, cremaster, and cheek pouch (28), and they contribute significantly to the regulation of peripheral blood flow (6). Small veins or large venules serve primarily as capacitance vessels. Whereas the responses of the arteriolar network has been extensively studied, such studies have focused on the behavior of the smaller vessels, i.e., <50 μm in diameter. However, it has been shown in hypertensive rats that large arterioles and small arteries, and not small arterioles, are responsible for a major increase in total organ vascular resistance (2).

The microcirculation exhibits different but specific physiological responses in each microvessel type, including the resistance vessels (inner diameter 100–1,600 μm) and capacitance vessels (150–250 μm) to the adrenoreceptor agonists, pH, endothelium-derived relaxig factor (EDRF), metabolism, etc. (9, 11, 12, 23). Because these conclusions were derived from studies performed under anesthesia or were inferred from in vitro studies, it is not clear whether such findings would also pertain to conscious animals. Slaaf et al. (37) and Davis (4) studied resistance and capacitance vessels in the intact unanesthetized bat wing preparation, although they studied arterioles <50 μm. Fenger-Gron et al. (10) recently reported the noninvasive measurement of intestinal blood flow in resistance arteries by implanting a catheter and a pulsed Doppler flow probe (outer diameter 500–1,000 μm), where blood flow was estimated under the assumption that vessel diameter did not change during the procedure.

In previous studies from our laboratory dealing with shock and hemodilution using the unanesthetized hamster dorsal skinfold preparation, we found contradictory phenomena: microvascular blood flow decreased significantly even though arteriolar diameters did not constrict enough to explain the decreased blood flow (19, 34). Those studies were carried out with the hamster chamber window model (7) to examine microvascular perfusion in unanesthetized conditions by intravital microscopy (13, 31), in which the glass window was usually implanted on the dorsal skin in such a manner that the diameter of the largest arteriole observed (A_1) is ~60 μm, and that of the largest venule observed (V_L) is ~100 μm (19, 29). To explore the hemodynamics upstream and downstream from the A_1 and V_L vessels, we installed the glass window in such fashion that a paired small artery (A_0, diameter, 156 ± 23 μm) and a small vein (V_0, 365 ± 64 μm) were present in the window. This modified hamster skinfold model was used to study the diameter, blood flow rate, and oxygen tension of A_0 and V_0 vessels in combination with the conventional observation of the downstream microvasculature, during resuscitation from hemorrhagic shock with human serum albumin (HSA) and shed

The costs of publication of this article were defrayed in part by the payment of page charges. The article must therefore be hereby marked "*advertisement*" in accordance with 18 U.S.C. Section 1734 solely to indicate this fact.

autologous blood (SAB). Intravascular oxygen tension measurements were used to determine whether the observed responses were due to local oxygen regulation or mediated through other mechanisms. We selected HSA as a plasma expander that closely reproduces the characteristics of natural plasma. Our aim was to determine whether the behavior of the larger vessels could explain the decreased flow during hemorrhage and its recovery during resuscitation.

MATERIALS AND METHODS

Animal model and preparation. Experiments were carried out in 20 male Syrian golden hamsters of 66 ± 8 g body wt (Simonsen, Gilroy, CA). All animals were housed in cages and provided with food and water ad libitum in a temperature-controlled room on a 12:12-h dark-light cycle. With each rat under pentobarbital sodium anesthesia (100 mg/kg body wt ip, Abbott, North Chicago, IL), the dorsal skinfold consisting of two layers of skin and muscle was fitted with two titanium frames with a 15-mm circular opening and surgically installed as shown in Fig. 1. A location that included a paired small artery and vein was selected. Layers of skin muscle were separated from the subcutaneous tissue and removed until a thin monolayer of muscle including the small artery and vein and one layer of intact skin remained. A cover glass (diameter, 12 mm) held by one frame covered the exposed tissue allowing intravital observation of the small artery (diameter, 156 ± 23 μm) and vein (365 ± 64 μm) which run in parallel. These are the main feeding and collecting vessels in the tissue.

Polyethylene tubes (PE-10, 1 cm; Becton Dickinson, Parsippany, NJ) were connected to a PE-50 tube (25 cm) via silicone elastomer medical tubes (4 cm, Technical Products) and were implanted in the jugular vein and the carotid artery. They were passed from the ventral to the dorsal side of the neck and exteriorized through the skin at the base of the chamber. The patency of the catheters was ensured by filling with heparinized saline (40 IU/ml).

Microvascular observations of the awake and unanesthetized hamsters were performed at least 5 days after chamber implantation to mitigate postsurgical trauma. During the measurements the animals were placed in a perforated plastic tube (inner diameter, 3.8 cm; length, 17 cm), from which the window chamber protrudes, to minimize animal movement without impeding respiration.

A preparation was considered suitable for experimentation if microscopic examination of the window chamber met the criteria of no sign of bleeding and/or edema, and the diameter of the resistance vessel was >130 μm.

All animal studies were approved by the Animal Subject Committee of University of California, San Diego, and the National Institutes of Health *Guide for the Care and Use of Laboratory Animals* [DHHS Publication No. (NIH) 85-23, Revised 1985] principles have been observed.

Resuscitation from hemorrhagic shock. Hemorrhagic shock was induced by bleeding 50% of the blood volume from the carotid artery in 5 min. Systemic blood volume was estimated as 7% of the total body weight. Blood was withdrawn into a heparinized syringe and stored for 45 min at room temperature. It was not refrigerated because of the short period, thus avoiding the need for rewarming before injection and potential complications due to platelet activation at a low temperature. Mean arterial pressure (MAP) was maintained at ~40 mmHg for 45 min through additional withdrawals in the range of 0.2–0.9 ml. Twenty hamsters were hemorrhaged and four hamsters died during the period of hypotension. Survivors were resuscitated with either SAB (n = 8) or 8% HSA (n = 8) in 5 min. The 8% HSA solution was prepared by dilution of 25% HSA solution (Bayer) with saline. Systemic and microhemodynamic parameters and blood gas parameters were evaluated before hemorrhage (baseline), after 50% hemorrhage, before resuscitation, just after resuscitation, and 0.5, 1.0, 1.5, and 2 h after resuscitation. The in situ

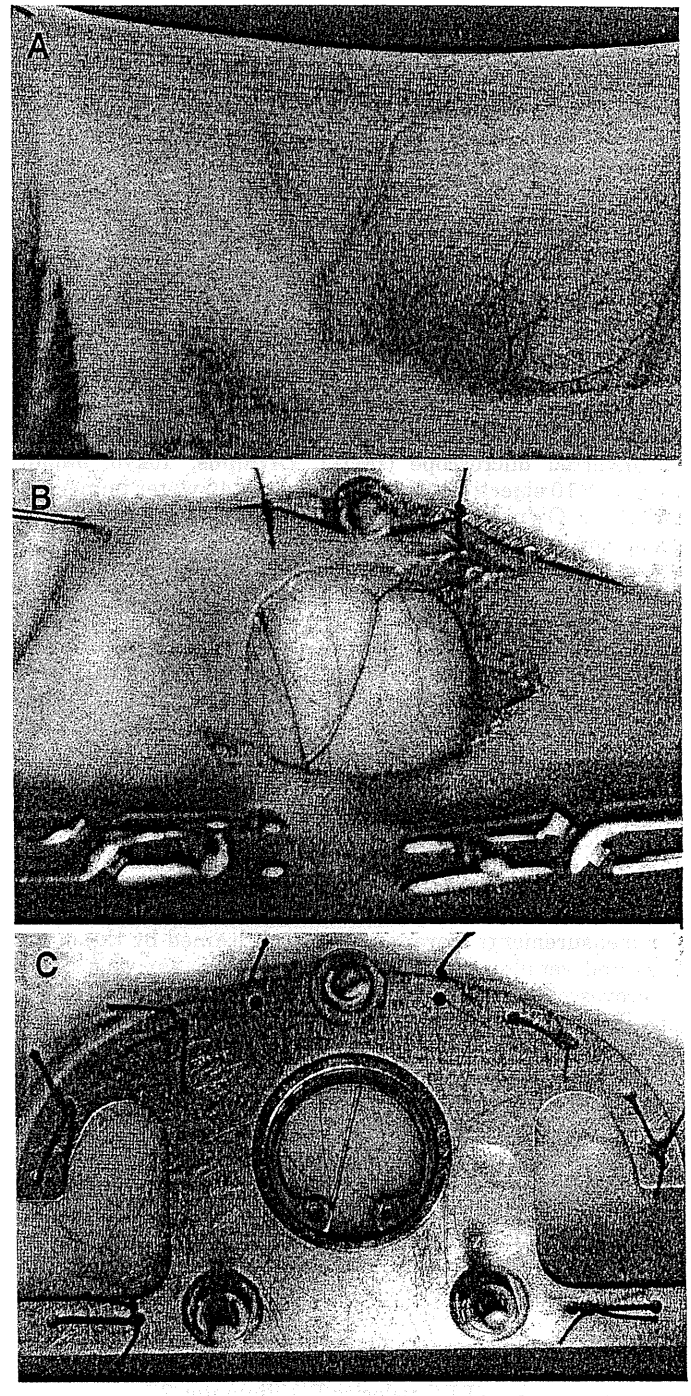

Fig. 1. Surgical procedure of the installation of a glass window on a hamster dorsal skin. *A*: hamster dorsal skin was pulled up to show semitransparently the Y-shaped (sometimes T-shaped) small artery and vein. *B*: layers of skin and muscle on one side were removed until a thin monolayer of muscle and one layer of intact skin remained with the small artery and vein. *C*: cover glass on a frame was installed to the exposed tissue.

microcirculation of the skinfold chamber was observed using a video-microscope system. After 2 h from resuscitation, palladium-porphyrin bound to bovine albumin solution (7.6 wt%, 0.1 ml) was injected intravenously to measure oxygen tension (Po_2) in vessels and interstitium (18, 40).

Characterization of systemic conditions. Blood samples were collected in heparinized microtubes (<100 μl, Curtin Matheson Scientific, Norcross, GA) for hematocrit and blood gas analyses. A pH/blood gas analyzer (model 248, CHIRON Diagnostics, Halstead, UK) was used for analysis of arterial blood oxygen tension (Pa_{O_2}), arterial blood carbon dioxide tension (Pa_{CO_2}), and pH. An analog recording system (Beckman R611, Beckman Instruments, Schiller Park, IL) was used for continuous monitoring of MAP and heart rate (HR).

Microhemodynamic analysis. Microvessels in the subcutaneous tissue and the skeletal skin muscle were observed with an inverted microscope (IMT-2, Olympus, Tokyo, Japan) using a ×10 objective (Olympus) and a ×40 water immersion objective (Olympus, Wplan) and transillumination. Microscopic images were recorded by video (Cohu 4815–2000, San Diego, CA) and transferred to a TV-VCR (Sony Trinitron PVM-1271Q monitor, Tokyo, Japan) and Panasonic AG-7355 video recorder (Tokyo, Japan). Microvessels were classified by their position within the microvascular network according to the previously reported scheme (17). Arteriolar microvessels were grouped into small arteries (A_0, diameter 156 ± 23 μm), large feeding arterioles (A_1, 59.5 ± 11.0 μm), small arcading arterioles (A_2, 25.6 ± 6.4 μm), transverse arterioles (A_3, 10.2 ± 2.5 μm), and terminal arterioles (A_4, 8.6 ± 1.8 μm). Venules were classified as small collecting venules (V_C, 25.9 ± 4.6 μm), large venules (V_L, 79.7 ± 15.3 μm), and small veins (V_0, 365 ± 64 μm). The microvessels selected for measurements were chosen for their optical clarity and not for the nature of their flow. Capillaries and tissue segments selected for measurements were supplied and drained by the arterioles and venules of a functional microvascular unit. These microvessels and capillaries were sketched in advance to plan the sequence of measurements. Selection of vessels in terms of visibility may bias the measurements in the direction of high flow value; however, because the same vessels were measured throughout the study, the trends observed should be representative for the microcirculation in this tissue.

Microvascular diameter and centerline red blood cell (RBC) velocity were analyzed on-line in arterioles and venules (14, 15). Vessel diameter was measured with an image-shearing system (Digital Video Image Shearing Monitor 908, IPM, San Diego, CA), whereas RBC velocity was analyzed by photodiodes and the cross-correlation technique (Velocity Tracker Mod-102 B, IPM). Blood flow rates ($\dot{Q}$) were calculated by means of the following

$$\dot{Q} = (\text{RBC velocity}/R_v)(\text{diameter}/2)^2 \quad (1)$$

where R_v represents the ratio of velocity in the middle of vessels to whole blood velocity based on the data in the glass tubes. According to Lipowsky and Zweifach (24), R_v equaled 1.6 for larger vessels with diameters >17 μm, and R_v equaled 1.3 for narrower vessels with diameters <10 μm. Therefore, R_v at 1.6 was used for A_0, A_1, A_2, V_C, V_L, and V_0, and R_v at 1.3 was used for A_3 and A_4.

Functional capillary density was analyzed on-line by counting the number of capillaries with RBC flow stemming from one A_3 arteriole, usually ~40–80 capillaries and expressed as a percentage of the basal value.

Determination of microvascular and interstitial Po_2. Subcutaneous microvascular and interstitial Po_2 was determined by the method of oxygen-dependent quenching of phosphorescence emitted by bovine serum albumin-bound metalloporphyrin complexes after pulsed light excitation (18, 40). This technique provides a noninvasive measurement of intravascular Po_2 and determination of interstitial oxygenation, because intravascularly injected porphyrin complexes bound to albumin extravasate into the interstitium over time. The relationship between phosphorescence lifetime τ and Po_2 is given by the Stern-Volmer equation

$$\tau_0/\tau = 1 + k_q \times \tau_0 \times Po_2 \quad (2)$$

where τ_0 and τ are the phosphorescence lifetimes in the absence of molecular oxygen and at a given Po_2, respectively, and k_q is the quenching constant, both factors being pH and temperature dependent. Palladium-*meso*-tetra(4-carboxyphenyl)porphyrin (Porphyrin Products, Logan, UT) bound to bovine serum albumin (Sigma, St. Louis, MO) was diluted with saline to a final concentration of 7.6 wt% (τ_0 = 600 μs, k_q = 325 $Torr^{-1} \cdot s^{-1}$, at pH = 7.4, and 37°C) and injected intravenously (0.1 ml). Phosphorescence was excited by light pulse (30 Hz) generated by a 45-W xenon strobe arc (EG&G Electro Optics, Salem, MA), and Po_2 measuring sites were microscopically vignetted by an adjustable slit. For intravascular Po_2 measurements, the slit was longitudinally fitted within the vessel, whereas for the analysis of interstitial Po_2, it was placed in intercapillary spaces, avoiding interference with blood vessels. Filters of 420 and 630 nm were used for porphyrin excitation and phosphorescence emission, respectively. Phosphorescence signals were captured by a photomultiplier (EMI 9855B, Knott Elektonik, Munich, Germany). In total, 128 decay curves were averaged, visualized, and saved by a digital oscilloscope (Hitachi Oscilloscope V-1065, 100 MHz, Hitachi Denshi, Tokyo, Japan). Decay time constants were determined by computer fitting the averaged decay curves to a single exponential, using the Stern-Volmer equation, and predetermined parameters of τ and k_q were corrected for the prevailing systemic blood pH and temperature (29°C) in the window chamber. Because in anemia pH may be lower than the systemic value and considering that the quenching time constant increases by 8% as pH varies from 7.20 to 6.20, interstitial Po_2 may be slightly overestimated.

Microvascular Po_2 measurements were made 10 min after dye injection to allow for its uniform dispersion into the vascular compartment, starting with measurements in the vessels, because these initially contain most of the dye. The reflection coefficient for albumin in subcutaneous connective tissue is in the range of 0.8–0.9, causing a natural and continuous steady extravasation of albumin, which yields a measurable steady-state concentration of the albumin-bound porphyrin complex in the tissue within 20–30 min. The material usually appears to be evenly distributed in the interstitium, because there is no evidence of significant variability in signal strength in the interstitium after the initial equilibration of 20–30 min. After the diffusion of the dye, Po_2 is not measured in vessels because signals arising from the dye in the overlying tissue may combine with those originating from blood yielding unreliable data. To circumvent this problem, Po_2 are measured only once at control and each time point in a hamster group. In the hemorrhage experiments control values were obtained for each group for diameters and blood flow. An additional group of animals (13 hamsters, 68 ± 7 g) was used to obtain the control values for Po_2.

Data analysis. Data are expressed as means ± SD for the indicated number of animals. Data between treatment groups were analyzed using a one-way ANOVA followed by Fisher's protected least significant difference test. A paired *t*-test was used to compare the time-dependent changes within each

group. The changes were considered statistically significant if $P < 0.05$.

RESULTS

Systemic responses. MAP of the SAB and HSA groups before hemorrhage was 99 ± 8 and 102 ± 12 mmHg, respectively, and declined to ~40 mmHg, a level maintained for 45 min (Fig. 2). Immediately after resuscitation, the SAB group recovered to 100 ± 8 mmHg, which tended to gradually decrease to 87 ± 10 mmHg after 2 h, which was significantly lower than the baseline value. The MAP in the HSA group was 58 ± 19 mmHg after resuscitation and slowly rose to a maximum after 1 h to 75 ± 8 mmHg and then tended to decrease. The SAB group had significantly higher MAP than the HSA group at all time points after resuscitation.

In both the SAB and HSA groups, HR significantly fell during hemorrhagic shock. Although the SAB group did not show an immediate recovery, HR returned to 531 ± 91 beats/min after 0.5 h (baseline, 462 ± 78 beats/min). HR in the HSA group did not recover and was significantly lower than in the SAB group after 0.5, 1.0, and 1.5 h.

Hematocrit before hemorrhage was 47–49% and was reduced to ~32% after shock due to the compensatory increase in plasma volume. After resuscitation, the hematocrit in the SAB group increased to 41.8 ± 2.2%, whereas the hematocrit in the HSA group was reduced to 15.7 ± 1.1% due to the dilution with the HSA solution.

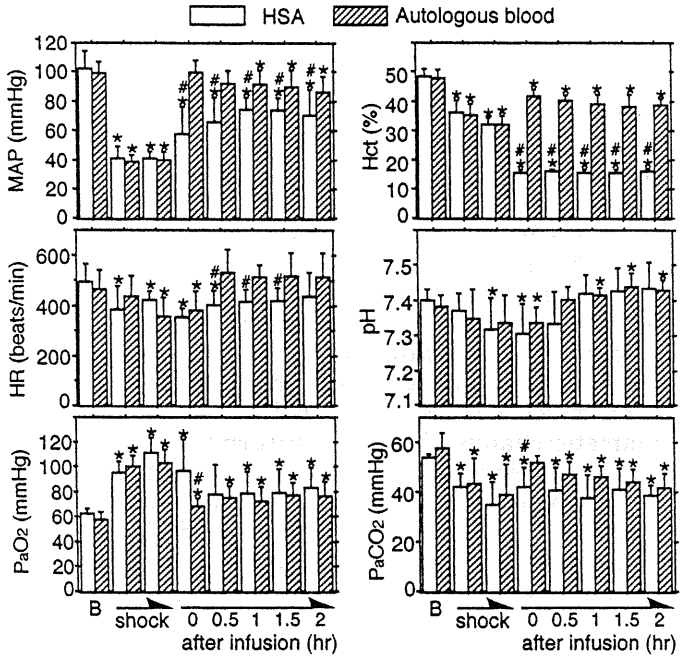

Fig. 2. Changes in systemic parameters from basal values during hemorrhagic shock and after resuscitation with human serum albumin (HSA) or shed autologous blood (SAB). Values are means ± SD. *Significantly different from baseline ($P < 0.05$); #significantly different between two groups ($P < 0.05$). B, baseline; MAP, mean arterial pressure; HR, heart rate; Pa_{O_2}, arterial blood oxygen tension; Pa_{CO_2}, arterial blood carbon dioxide tension; Hct, hematocrit.

Table 1. *Basal values of vessel diameter, centerline red blood cell velocity, and calculated flow rate of observed blood vessels for the experiment and intravascular oxygen tensions in the normal condition*

Microvessels	Diameter, μm	Velocity, mm/s	Flow Rate, nl/s	P_{O_2}, mmHg
A_0	156 ± 23	33.5 ± 7.4	394 ± 133	53 ± 3
A_1	59.5 ± 11.0	10.2 ± 4.4	19.6 ± 13.7	50 ± 3
A_2	25.6 ± 6.4	7.6 ± 4.8	2.52 ± 2.30	47 ± 7
A_3	10.2 ± 2.5	4.5 ± 2.2	0.31 ± 0.24	42 ± 4
A_4	8.6 ± 1.8	2.3 ± 1.1	0.11 ± 0.09	39 ± 5
V_C	25.9 ± 4.6	1.0 ± 0.5	0.36 ± 0.22	33 ± 9
V_L	79.7 ± 15.3	2.9 ± 1.4	9.58 ± 6.11	35 ± 6
V_0	365 ± 64	7.4 ± 2.8	443 ± 216	37 ± 2

Values are means ± SD ($n = 20$ hamsters, 66 ± 8 g body wt for basal values). P_{O_2} measurements were made only once in each group of animals, because they cannot be repeated after the dye has diffused into the tissue; therefore, whereas diameter and blood flow control values could be established for each resuscitation group, control P_{O_2} values were obtained from a separate group of 13 hamsters (68 ± 7 g body wt).

Hamsters in the normal condition at baseline had relatively lower Pa_{O_2} (58.7 ± 5.5 mmHg) and higher Pa_{CO_2} (55.7 ± 3.8 mmHg) than the other animals due to the alveolar hypoventilation, a result from their adaptation to a fossorial environment (30). Hemorrhagic shock induced typical hyperventilation, which significantly increased Pa_{O_2} to 106.1 ± 12.2 mmHg and decreased Pa_{CO_2} to 38.8 ± 9.7 mmHg, and significant metabolic acidosis occurred as shown by the decrease in pH from 7.39 ± 0.03 to 7.33 ± 0.09. The SAB group immediately recovered from the hyperventilation after resuscitation, showing Pa_{O_2} of 68.4 ± 5.9 mmHg and Pa_{CO_2} of 51.8 ± 2.8 mmHg. The HSA showed a decrease in Pa_{O_2}, which was 77.8 ± 23.8 mmHg 0.5 h after resuscitation. Both groups remained slightly hyperventilated after 0.5 h with significant differences in comparison with baseline values. Pa_{CO_2} of the HSA group, however, remained at nonsignificantly lower values than those of the SAB group throughout resuscitation. Both groups tended to increase pH to >7.40, indicating respiratory alkalosis.

Characteristics of classified microvessels. Table 1 shows the basal value of diameter, centerline RBC velocity, blood flow rate, and P_{O_2} of each microvessel. A_0 and V_0 showed centerline RBC velocities of 33.5 ± 7.4 and 7.4 ± 2.8 mm/s, respectively, and blood flow rates of 394 ± 133 and 443 ± 216 nl/s, respectively. P_{O_2} in A_0 was 53 ± 3 mmHg, decreasing to 39 ± 5 mmHg in A_4 arterioles. This reduction is due to the diffusion of oxygen from arterioles (13). Mean P_{O_2} in venules increased slightly from 33 ± 9 mmHg in V_C to 37 ± 2 mmHg in V_0 due to the presence of convective and diffusive oxygen shunts.

Microhemodynamic responses. The hemorrhagic shock period in both the SAB and HSA group induced significant constrictions of A_0 (52% of the basal value), A_1 (82%), and V_0 (70%) and a tendency for dilation of A_2 (104%) and A_3 (117%) (Fig. 3). A_4, V_C, and V_L did not show specific diameter changes. The micrographs in Fig. 4 illustrate vasoconstriction of a small artery and

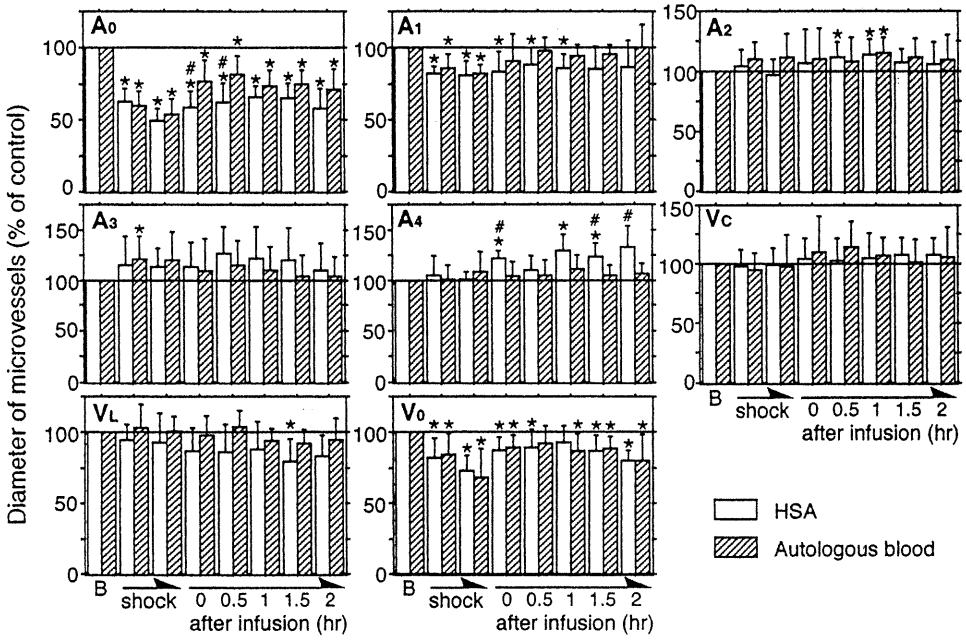

Fig. 3. Changes in diameter of small artery (A_0) and vein (V_0), arterioles (A_1, A_2, A_3, A_4), and venules (collecting and large, V_C and V_L, respectively) from basal values during hemorrhagic shock and after resuscitation with HSA or SAB. Values are means ± SD. B, baseline. *Significantly different from baseline ($P < 0.05$); #significantly different between two groups ($P < 0.05$).

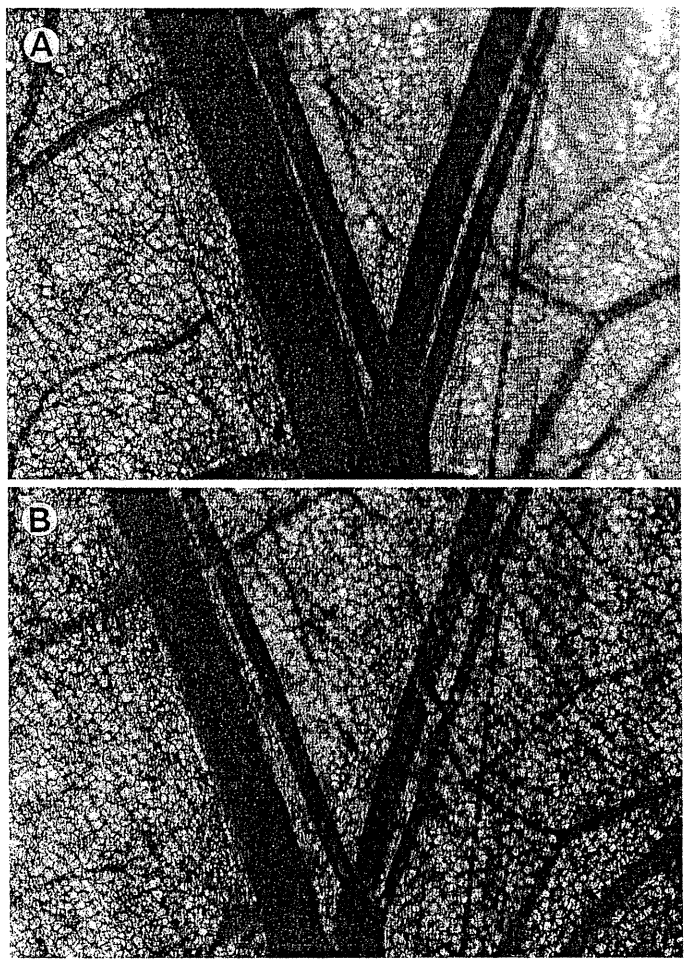

Fig. 4. Micrographs of a set of small artery and small vein before (*A*) and after (*B*) 45 min of hemorrhagic shock, indicating that these vessels significantly constricted.

vein pair. After resuscitation, the diameter of A_1 vessels in the SAB group returned close to the baseline value, and it was not statistically different from control, whereas the diameters of A_0 and V_0 did not return to the basal values and remained significantly lower even after 2 h (A_0, 71 ± 14%; V_0, 81 ± 18%). A_2 and A_3 tended to remain dilated with a significant dilation of A_2 at 1 h (115 ± 13%), whereas A_4, V_C, and V_L microvessels did not show specific changes after SAB infusion. There was a significantly smaller recovery of the A_0 diameter in the HSA group after resuscitation (59 ± 11%) than in the SAB group at 0 and 0.5 h and a tendency to maintain more constriction than in the SAB group; the vessel remained <70% of baseline even 2 h after resuscitation. Both A_1 and V_L tended to maintain constriction at 86 ± 19% and 83 ± 15% of baseline, respectively, at 2 h and with significant constriction of V_L at 1.5 h (80 ± 16%). A_2 and A_3 tended to remain dilated, showing significant dilation of A_2 at 0.5 and 1 h. A_4 dilated after HSA infusion and were significantly larger than basal values at 0, 1, and 1.5 h and significantly larger than the SAB group at 0, 1.5, and 2 h (133 ± 21% at 2 h). V_C did not show significant diameter changes. V_0 did not return to the basal values and remained significantly constricted at 2 h (80 ± 7%).

Although diameter changes were heterogeneous, flow in all the vessels showed similar and significant decreases during the hemorrhagic shock period (Fig. 5) in A_0 (5% of the basal value on the average), A_1 (7%), A_2 (12%), A_3 (7%), A_4 (17%), V_C (8%), V_L (10%), and V_0 (8%), which increased after infusion of the resuscitating fluids. The SAB group showed generally higher recovery in blood flow, e.g., at 0 h in A_0 (SAB 47% vs. HSA 8%), A_1 (32% vs. 22%), A_2 (83% vs. 48%), A_3 (55% vs. 18%), A_4 (90% vs. 75%), V_C (54% vs. 22%), V_L (56% vs. 32%), and V_0 (56% vs. 31%), with significant differences at the following time points: A_0, all the time points; A_1,

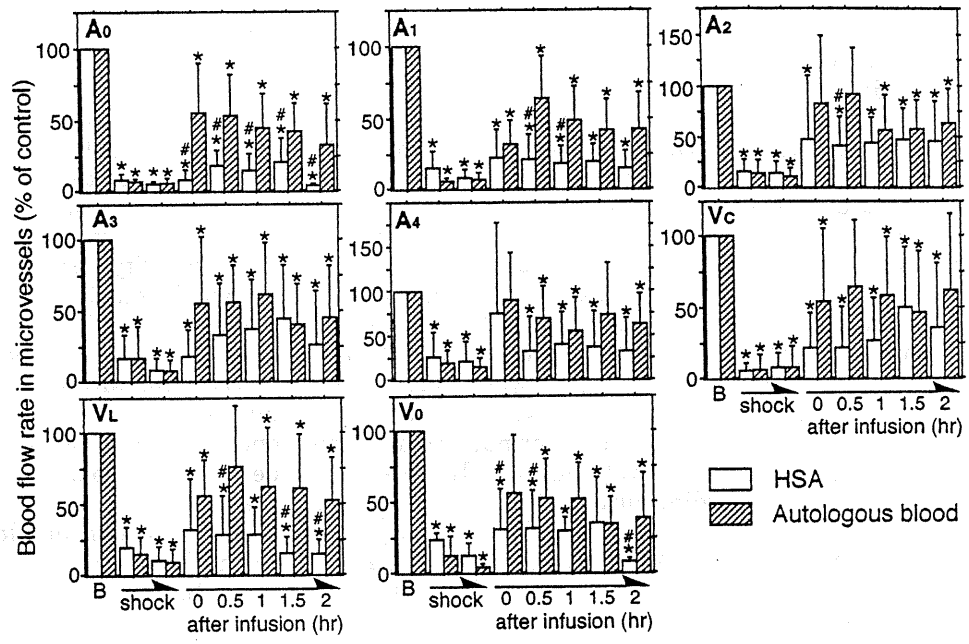

Fig. 5. Changes in blood flow rates in small artery (A_0) and vein (V_0), arterioles (A_1, A_2, A_3, A_4), and venules (V_C, V_L) from basal values during hemorrhagic shock and after resuscitation with HSA or SAB. Values are means ± SD. *Significantly different from baseline ($P < 0.05$); #significantly different between the two groups ($P < 0.05$).

0.5 and 1 h; A_2, 0.5 h; V_L, 0.5, 1.5, and 2 h; and V_0, 0, 0.5, and 2 h. However, flow in the SAB group on the average did not recover to the basal values even after 2 h.

Functional capillary densities of both the SAB and HSA groups diminished after the hemorrhagic shock period to 18% of the basal values (Fig. 6). The SAB group showed an immediate recovery to 75 ± 15% at 0 h, whereas the HSA group was 25 ± 21% and remained below 40% throughout the observation period. Both groups remained at significantly smaller values than the baseline.

Intravascular and interstitial oxygen tensions of the SAB group were nonsignificantly lower than the basal values, except in V_L, although significantly higher than the HSA group except for A_0 vessels. However, intravascular total oxygen content of A_0 of the HSA group was significantly lower than that of the SAB group due to the significantly lower hematocrit (16%); consequently the reduction of downstream P_{O_2} was significant.

DISCUSSION

One of the principal findings of this study is that only small arteries with diameters of ~160 μm and veins of ~370 μm constrict significantly with hemorrhage and remain significantly constricted during resuscitation in the nonanesthetized, intact hamster window preparation. These vessels correspond to branches of the circumflex scapula artery and vein in humans (8) and are located outside of both the skin and muscle. The same kind of vessels in the hamster cremaster muscle and the rat hindlimb muscle preparations were termed "feed arteries" and were reported to regulate blood flow to a significant degree (36, 44). Meininger et al. (27) studied the anatomic arrangement, pressure distribution, and resting vascular tone of feed arteries located upstream from the rat cremaster microcirculation and demonstrated that small arteries of ~140 μm in diameter showed the largest pressure drop of any vascular order.

These blood vessels occupy a special niche within the vasculature in terms of their experimental access, because they are too small to be analyzed by conventional systemic hemodynamic techniques, and con-

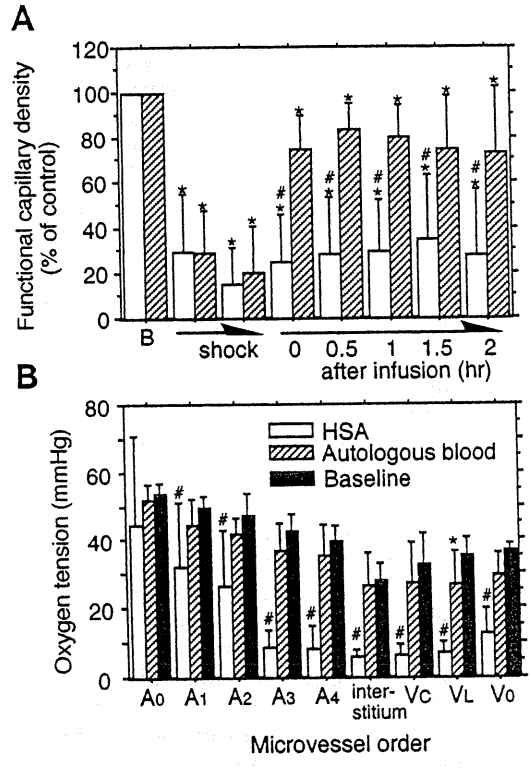

Fig. 6. *A*: changes in functional capillary density from basal values during hemorrhagic shock and after resuscitation with HSA or SAB. Values are means ± SD. *Significantly different from baseline ($P < 0.05$); #significantly different between two groups ($P < 0.05$). *B*: intravascular and interstitial oxygen tensions 2 h after resuscitation in comparison with basal values. #Significantly different from the baseline and SAB group ($P < 0.05$); *significantly different from baseline ($P < 0.05$).

versely they tend to be outside the scope of most microvascular studies and methods. Most previous reports dealing with resistance arteries focus on their reactivity in terms of diameter changes; however, in the hamster skinfold preparation, the tissue is sufficiently transparent to allow measurement of RBC velocity with photodiodes and the cross-correlation technique. Blood flow velocity in these small arteries under normal conditions was 33.5 ± 7.4 mm/s (among the fastest velocity measured with the cross-correlation method) corresponding to a blood flow rate of 394 ± 133 nl/s.

Volume flow in the tissue under study fell to 5–17% of control levels when arterial pressure was reduced to 40 mmHg. This large reduction in flow is in part due to the low MAP and the decline in cardiac output as evidenced by the decreased vascular volume and HR. We were unable to measure cardiac output of the hamsters due to the small body weight (60 g). Cardiac output is reported to fall as much as 50% in hemorrhage (22, 32, 35); however, it is unlikely that it would be reduced to <20% of control, therefore, the decrease in flow in this tissue evidences a significant redistribution of vascular resistance, attributable to the changes in vascular diameter observed in the small arteries and to a lesser degree in the small veins. This suggests that the "centralization" of blood flow in hemorrhage may be controlled by these resistance vessels.

The finding that small arteries and veins are the principal effectors of increased vascular resistance in shock and/or extreme hemodilution explains previous findings from this laboratory showing the significant reductions of blood flow in the absence of notable changes in microvascular vessel caliber. The difference in response between large and smaller microvessels during hemorrhagic shock has been reported in previous studies (3, 17, 19), which found significant constrictions of large arterioles and dilation of precapillary arterioles in conscious hamster dorsal skin. A similar result was found when MAP decreased in the anesthetized and exteriorized cat sartorius muscle (39) and rat cremaster muscle (46). In general, however, the level of constriction found in the larger arterioles was not sufficient to explain the significant reduction of blood flow, suggesting that more significant changes may occur in larger vessels.

Our findings fully support the contention that during hemorrhagic shock, active regulation occurs primarily at the level of the small A_0 arteries and the small V_0 veins. Furthermore, our results demonstrate that interpretation of microvascular events is critically linked to information about the hierarchical distribution of microvessels in the network. In our study, network location fully accounts for the heterogeneous microvascular responses, and vessel reactions follow a defined pattern. As an example, the arcading arterioles A_2 tended to remain at basal values or dilated at all time points after resuscitation from hemorrhagic shock, whereas A_0 and V_0 vessels did not return to the basal value even after resuscitation with SAB.

The time course of change in blood flow in all microvessels and that of functional capillary density, which were significantly reduced during the shock period and increased after resuscitation, also coincided with the diameter changes of the small A_0 arteries and not the remainder of the arteriolar vessels. The SAB group showed higher and faster responses than the HSA group. In terms of Poiseuille's law, blood flow in a tube is proportional to the fourth power of the radius, the pressure gradient, and inversely proportional to fluid viscosity. Assuming that A_0 dominates the downstream blood flow and considering a reduction of A_0 diameter to 80% of the basal value, the reduced blood viscosity due to the reduced hematocrit (ca. 40% for the SAB group, initially 50%), and the reduced MAP, which may affect the regional arteriovenous pressure difference (ca. 90%), then the reduction in blood flow rate can be estimated to be $(0.8)^4 \times 50/40 \times 0.9 \times 100 = 46\%$ of the basal value. This estimate corresponds to our finding on the incomplete recovery of blood flow rates of the SAB group shown in Fig. 5. This calculation indicates that the reactivity of the A_0 small arteries is crucial in determining conditions in the downstream microcirculation.

Normally intravascular P_{O_2} decreases from A_0 (53 ± 3 mmHg) to A_4 (39 ± 5 mmHg). This reduction is due to oxygen diffusion from arterioles and consumption by the vascular wall (13, 41). Tissue P_{O_2} is 28 ± 5 mmHg and blood P_{O_2} increases after passing through the capillaries being 33 ± 9 mmHg in V_C and 37 ± 3 mmHg in V_0 due to the presence of diffusive and convective shunts between arterioles and venules. Two hours after resuscitation, P_{O_2} in vessels of the SAB group were not significantly lower than basal values, although blood flow was reduced and were significantly higher than the HSA group in A_2, A_3, A_4, V_C, V_L, and V_0 vessels. P_{O_2} in A_0 vessels of the HSA group was 44 mmHg, whereas most of the oxygen exited the arterioles before blood entered the capillaries. The low intravascular P_{O_2} values are also a consequence of the decreased blood oxygen-carrying capacity due to the low hematocrit and the diffusion from arterioles before blood enters the capillaries. This phenomenon may be enhanced by the reduced blood flow rate, which may provide additional time for oxygen to diffuse from RBCs to the vascular walls. As a result, P_{O_2} values in A_3, A_4, V_C, and V_L are <10 mmHg on the average.

Our finding may in part be due to nonuniformity of the sympathetic innervation in small arteries and arterioles (12). Normally, α_1-receptors are located only in larger arterioles and venules, and α_2-receptors are located throughout the arteriolar and venular microvasculature (9). The primary compensation to acute hemorrhagic shock includes release of adrenal catecholamines, although norepinephrine (α_2-receptor agonist)-mediated constriction of small terminal arterioles is reduced by a metabolic acidosis (26) and hypoxia (23). In cat sartorius muscle, the escape from sympathetic stimulation is due to a fall in parenchymal cell P_{O_2} and not periarteriolar P_{O_2} (1). Dilation of small arterioles in the hamster cheek pouch during systemic hypotension was reported to be abolished by elevated suffusate P_{O_2} (25). These observations suggest that the escape from

constriction of small arterioles during hemorrhagic shock and resuscitation, such as A_4 vessels in the HSA group, may be due to the impaired oxygenation of the microvasculature as shown by the significantly lower P_{O_2} levels throughout the microvessels in the tissue. Furthermore, the prevalent constriction of the A_0 vessels during shock and resuscitation should reduce hydraulic pressure in the subsequent vessels, which may tend to dilate according to myogenic responses (16). Consequently the lack of constriction in the smaller vessels may be due to the combined effect of two local autoregulatory processes that oppose the constrictor stimulus.

The difference in the recovery of blood flow, oxygenation, and functional capillary density between HSA and SAB may not only be due to oxygen content but also due to the viscosity of the circulating blood and the heterogeneous shear stress-dependent production of EDRF. Griffith et al. (11) showed that rabbit ear small arteries (diameter range: 150–700 μm), where resistance and shear stress are maximal, have the highest EDRF sensitivity. EDRF-mediated shear-induced dilation of arterioles and small arteries has been extensively studied (21, 33, 38). Shear stress on the wall is given by $(4 \cdot \eta \cdot \dot{Q})/(\pi r^3)$, where η is viscosity, $\dot{Q}$ is blood flow rate, and r is the radius. Blood viscosity was determined with a capillary viscometer (42) requiring only a 0.4-ml sample for measurements at an average shear rate of 119 s^{-1}. Circulating blood viscosities after infusion of autologous blood and HSA were 4.0 and 1.6 cP, respectively (intact blood: 4.5 cP). This would reduce shear stress in A_0 arteries by 50% during resuscitation in the SAB group and 90% in the HSA group if the diameter is maintained and may be related to the significant differences in A_0 vessels diameters (45) and functional capillary density between groups.

Other studies of hemorrhagic shock have shown that the fraction of cardiac output distributed to dermal, renal, and splanchnic beds declines, whereas the fraction distributed to brain and myocardium increases (20, 35), a phenomenon termed "centralization." The constriction of the resistance arteries may serve to sustain blood pressure, and constriction of the capacitance vessels may enhance blood redistribution from the skin to the vital organs. In summary, this study demonstrates the central role of resistance arteries in reducing blood flow in hemorrhagic shock and resuscitation, a phenomenon that has a significant impact on peripheral vascular resistance and may contribute to the blood centralization.

The authors acknowledge the contribution of Dr. Shunichi Usami for evaluating the viscometry data and Dr. Dominique Erni for suggesting the surgical technique.

This work has been supported in part by a National Heart, Lung, and Blood Institute Program Project (HL-48018); Grants-in-Aid for Scientific Research from the Ministry of Education, Science, Sports and Culture, Japan (07508005); and Health Science Research Grants (Artificial Blood Project) from the Ministry of Health and Welfare, Japan. H. Sakai was an overseas research fellow of the Japan Society for the Promotion of Science (1996–1997) and is a research resident of the Japan Health Sciences Foundation (1998).

Addresses for reprint requests and correspondence: M. Intaglietta, Dept. of Bioengineering, University of California, San Diego, 9500 Gilman Dr., La Jolla, CA 92093-0412; E. Tsuchida, Dept. of Polymer Chemistry, Advanced Research Institute for Science and Engineering, Waseda Univ., Tokyo 169-8555.

Received 13 April 1998; accepted in final form 20 October 1998.

REFERENCES

1. **Boegehold, M. A., and P. C. Johnson.** Periarteriolar and tissue P_{O_2} during sympathetic escape in skeletal muscle. *Am. J. Physiol.* 254 (*Heart Circ. Physiol.* 23): H929–H936, 1988.
2. **Bohlen, H. G.** Localization of vascular resistance changes during hypertension. *Hypertension* 8: 181–183, 1986.
3. **Colantuoni, A., S. Bertuglia, and M. Intaglietta.** Microvessel diameter changes during hemorrhagic shock in unanesthetized hamsters. *Microvasc. Res.* 30: 133–142, 1985.
4. **Davis, M. J.** Control of bat wing capillary pressure and blood flow during reduced perfusion pressure. *Am. J. Physiol.* 255 (*Heart Circ. Physiol.* 24): H1114–H1129, 1988.
5. **Davis, M. J., P. N. Ferrer, and R. W. Gore.** Vascular anatomy and hydrostatic pressure profile in the hamster cheek pouch. *Am. J. Physiol.* 250 (*Heart Circ. Physiol.* 19): H291–H303, 1986.
6. **Duling, B. R.** The role of the resistance arteries in the control of peripheral resistance. In: *Resistance Arteries: Structure and Function*, edited by M. J. Mulvany, C. Aalkjær, A. M. Heagerty, N. C. B. Nyborg, and S. Strandgraard. Oxford, UK: Elsevier Science, 1991, p. 3–9.
7. **Endrich, B., K. Asaishi, A. Götz, and K. Messmer.** Technical report–a new chamber technique for microvascular studies in unanesthetized hamsters. *Res. Exp. Med. (Berl.)* 177: 125–134, 1980.
8. **Erni, D. H. Sakai, A. G. Tsai, A. Banic, and M. Intaglietta.** The hamster island flap–a versatile model for investigating ischemia due to trauma and surgery by intravital microscopy (Abstract). *J. Vasc. Res.* 35, *Suppl.* 2: 74, 1998.
9. **Faber, J. E.** In situ analysis of α-adrenoreceptors on arteriolar and venular smooth muscle in rat skeletal muscle microcirculation. *Circ. Res.* 62: 37–50, 1988.
10. **Fenger-Gron, J., M. J. Mulvany, and K. L. Christensen.** Intestinal blood flow is controlled by both feed arteries and microcirculatory resistance vessels in freely moving rats. *J. Physiol. (Lond.)* 498: 215–224, 1997.
11. **Griffith, T. M., D. H. Edwards, R. L. Davies, and A. H. Henderson.** The role of EDRF in flow distribution: a microangiographic study of the rabbit isolated ear. *Microvasc. Res.* 37: 162–177, 1989.
12. **Hirata, S., and I. Ninomiya.** Nonuniform effects of sympathetic nerve and α-receptor blockade on internal diameter of small arteries in the rabbit ear. *Clin. Hemorheol.* 2: 229–241, 1982.
13. **Intaglietta, M., P. C. Johnson, and R. M. Winslow.** Microvascular and tissue oxygen distribution. *Cardiovasc. Res.* 32: 632–643, 1996.
14. **Intaglietta, M., N. R. Silverman, and W. R. Tompkins.** Capillary flow velocity measurements in vivo and in situ by television methods. *Microvasc. Res.* 10: 165–179, 1975.
15. **Intaglietta, M., and W. R. Tompkins.** Microvascular measurements by video image shearing and splitting. *Microvasc. Res.* 5: 309–312, 1973.
16. **Johnson, P. C.** The myogenic response. *News Physiol. Sci.* 6: 41–42, 1991.
17. **Kerger, H., D. J. Saltzman, M. D. Menger, K. Messmer, and M. Intaglietta.** Systemic and subcutaneous microvascular oxygen tension dissociation during 4-h hemorrhagic shock in conscious hamsters. *Am. J. Physiol.* 270 (*Heart Circ. Physiol.* 39): H827–H836, 1996.
18. **Kerger, H., I. P. Torres Filho, M. Rivas, R. M. Winslow, and M. Intaglietta.** Systemic and subcutaneous microvascular oxygen tension in conscious Syrian golden hamsters. *Am. J. Physiol.* 268 (*Heart Circ. Physiol.* 37): H802–H810, 1995.
19. **Kerger, H., A. G. Tsai, D. J. Saltzman, R. M. Winslow, and M. Intaglietta.** Fluid resuscitation with oxygen versus nonoxygen

carriers after 2-h hemorrhagic shock in conscious hamsters. *Am. J. Physiol.* 272 (*Heart Circ. Physiol.* 41): H525–H537, 1997.

20. **Koehler, R. C., R. J. Traystman, and M. D. Johnes, Jr.** Regional blood flow and O_2 transport during hypoxic and CO hypoxia in neonatal and adult sheep. *Am. J. Physiol.* 248 (*Heart Circ. Physiol.* 17): H118–H124, 1985.
21. **Koller, A., D. Sun, and G. Kaley.** Role of shear stress and endothelial prostaglandins in flow- and viscosity induced dilation of arterioles in vivo. *Circ. Res.* 72: 1276–1284, 1993.
22. **Kreimeier, U., U. B. Bruuckner, S. Niemczyk, and K. Messmer.** Hypertonic saline dextran for resuscitation from traumatic hemorrhagic hypotension: effect on regional blood flow. *Circ. Shock* 32: 83–99, 1990.
23. **Leech, C. J., and J. E. Faber.** Differential sensitivity of venular and arteriolar α-adrenergic receptor constriction to inhibition by hypoxia: role of receptor subtype and coupling heterogeneity. *Circ. Res.* 78: 1064–1074, 1996.
24. **Lipowsky, H., and B. Zweifach.** Application of the "two-slit" photometric technique to the measurement of microvascular volumetric flow rates. *Microvasc. Res.* 15: 93–101, 1978.
25. **Lombard, J. H., R. P. Kaminski, and W. J. Stekiel.** Arteriolar responses to changes in oxygen availability following single withdrawal hemorrhage. *Microvasc. Res.* 21: 332–342, 1981.
26. **McGillivray-Anderson, K. M., and J. E. Faber.** Effect of acidosis on contraction of microvascular smooth muscle by α_1- and α_2-adrenoreceptors. Implications for neural and metabolic regulation. *Circ. Res.* 66: 1643–1657, 1990.
27. **Meininger, G. A., K. L. Fehr, and M. B. Yates.** Anatomic and hemodynamic characteristics of the blood vessels feeding the cremaster skeletal muscle in the rat. *Microvasc. Res.* 33: 81–97, 1987.
28. **Mulvany, M. J., C. Aalkjær, A. M. Heagerty, N. C. B. Nyborg, and S. Strandgraard** (Editors). *Resistance Arteries: Structure and Function.* Oxford, UK: Elsevier Science, 1991.
29. **Nolte, D., A. Botzlar, S. Pickelmann, E. Bouskela, and K. Messmer.** Effects of diaspirin-crosslinked hemoglobin (DCLHb) on the microcirculation of striated skin muscle in the hamster: a study on safety and toxicity. *J. Lab. Clin. Med.* 130: 314–327, 1997.
30. **O'Brien, J. J., Jr., E. C. Lucey, and G. L. Sinder.** Arterial blood gases in normal hamsters at rest and during exercise. *J. Appl. Physiol.* 46: 806–810, 1979.
31. **Papenfuss, H. D., J. F. Gross, M. Intaglietta, and F. A. Treese.** A transparent access chamber for the rat dorsal skin fold. *Microvasc. Res.* 18: 311–318, 1979.
32. **Pascual, J. M. S., D. E. Runyon, J. C. Watson, C. B. Clifford, M. A. Dubick, and G. C. Kramer.** Resuscitation of hypovolemia in pigs using near saturated sodium chloride solution in dextran. *Circ. Shock* 40: 115–124, 1993.
33. **Pohl, U., K. Herlan, A. Huang, and E. Bassenge.** EDRF-mediated shear-induced dilation opposes myogenic vasoconstriction in small rabbit arteries. *Am. J. Physiol.* 261 (*Heart Circ. Physiol.* 30): H2016–H2023, 1991.
34. **Sakai, H., A. G. Tsai, H. Kerger, S. I. Park, S. Takeoka, H. Nishide, E. Tsuchida, and M. Intaglietta.** Subcutaneous microvascular responses to hemodilution with red cell substitutes consisting of polyethyleneglycol-modified vesicles encapsulating hemoglobin. *J. Biomed. Mater. Res.* 40: 66–78, 1998.
35. **Schlichtig, R., D. J. Kramer, and M. R. Pinsky.** Flow redistribution during progressive hemorrhage is a determinant of a critical O_2 delivery. *J. Appl. Physiol.* 70: 169–178, 1991.
36. **Sehgal, S. S., and B. R. Duling.** Communication between feed arteries and microvessels in hamster striated muscle: segmental vascular responses are functionally coordinated. *Circ. Res.* 59: 283–290, 1986.
37. **Slaaf, D. W., R. S. Reneman, and C. A. Wiederhielm.** Pressure regulation in muscle of unanesthetized bats. *Microvasc. Res.* 33: 315–326, 1987.
38. **Smiesko, V., D. J. Lang, and P. C. Johnson.** Dilator response of rat mesenteric arcading arterioles to increased blood flow velocity. *Am. J. Physiol.* 257 (*Heart Circ. Physiol.* 26): H1958–H1965, 1989.
39. **Torres, Filho, I. P., M. A. Boegehold, E. Bouskela, S. D. House, and P. C. Johnson.** Microcirculatory responses in cat sartorius muscle to hemorrhagic hypotension. *Am. J. Physiol.* 257 (*Heart Circ. Physiol.* 26): H1647–H1655, 1989.
40. **Torres, Filho, I. P., and M. Intaglietta.** Microvascular Po_2 measurements by phosphorescence decay method. *Am. J. Physiol.* 265 (*Heart Circ. Physiol.* 34): H1434–H1438, 1993.
41. **Tsai, A. G., B. Friesenecker, M. C. Mazzoni, H. Kerger, D. G. Buerk, P. C. Johnson, and M. Intaglietta.** Microvascular and tissue oxygen gradients in the rat mesentery. *Proc. Natl. Acad. Sci. USA* 95: 6590–6595, 1998.
42. **Usami, S., W. Reinhart, S. Danoff, and S. Chen.** A new capillary viscometer for measurements on small blood samples over a wide shear rate range. *Clin. Hemorheol.* 4: 295–297, 1984.
43. **Whitmore, R. L.** *Rheology of the Circulation.* Oxford, UK: Pergamon, 1968.
44. **Williams, D. A., and S. S. Segal.** Feed artery role in blood flow control to rat hindlimb skeletal muscle. *J. Physiol. (Lond.)* 463: 631–646, 1993.
45. **Wit, C., C. Schäfer, P. Bismarck, S.-S. Bolz, and U. Pohl.** Elevation of plasma viscosity induces sustained NO-mediated dilation in the hamster cremaster microcirculation in vivo. *Pflügers Arch.* 434: 354–361, 1997.
46. **Zhao, K.-S., D. Junker, F. A. Delano, and B. W. Zweifach.** Microvascular adjustments during irreversible hemorrhagic shock in rat skeletal muscle. *Microvasc. Res.* 30: 143–153, 1985.

Physicochemical Properties and O_2-Coordination Structure of Human Serum Albumin Incorporating Tetrakis(*o*-pivalamido)phenylporphyrinatoiron(II) Derivatives

Teruyuki Komatsu, Kazuyoshi Hamamatsu, Jian Wu, and Eishun Tsuchida*,†

Department of Polymer Chemistry, Advanced Research Institute for Science & Engineering, Waseda University, Tokyo 169-8555, Japan. Received July 16, 1998; Revised Manuscript Received October 12, 1998

Incorporation of tetrakis(*o*-pivalamido)phenylporphyrinatoiron(II) derivatives with a covalently linked axial imidazole (FeP) into human serum albumin (HSA) provides a new type of artificial hemoprotein (HSA-FeP) that binds and releases dioxygen reversibly under physiological conditions (in aqueous media, pH 7.4, 37 °C) and in a fashion similar to hemoglobin and myoglobin. The HSA host adsorbs a maximal eight FeP molecules, and their stepwise equilibrium constants (K_1–K_8) range from 1.2×10^6 to 1.3×10^4 M^{-1}. The major binding sites of the synthetic hemes are identical to those of hemin, bilirubin, and long-chain fatty acids. The red-colored solution of HSA-FeP was stored for three months at 4 °C and could be kept as a freeze-dried powder for more than six months. The solution properties [[HSA]: 5 wt %, FeP/HSA = 1–8 (mol/mol)] satisfy the physiological requirements for dioxygen infusion for potential clinical use; the specific gravity is 1.013, and the viscosity is 1.1 cP. Mixing the solution with human blood does not induce any coagulation and precipitation. On the basis of the gel permeation chromatography, CD spectroscopy, and IEF measurements, the molecular size, second-order structure, and surface charge distribution of the HSA-FeP conjugate are constant and independent of the binding numbers of heme molecules. Furthermore, the O_2-coordination structure of FeP embedded into certain hydrophobic domains of the albumin was confirmed by resonance Raman spectroscopy.

INTRODUCTION

In the bloodstream, serum albumin serves as a *shuttle* that transports an incredible variety of endogenous and exogenous compounds. Interest in this molecular binding led to research involving association studies of HSA with various ligands (Brown, 1976; Kragh-Hansen, 1981; Peters, 1975, 1985). Human serum albumin (HSA) was among the very first proteins crystallized in the microgravity environment of space (Carter et al., 1989, 1994; He et al., 1992). In contrast to the early conception of an oblate ellipsoid shape (140 × 40 Å), HSA is a unique heart-shaped molecule that can be approximated to be an equilateral triangle with sides of 8 nm and a depth of 3 nm. HSA has three homologue domains (I, II, and III) with nine loops formed by 17 disulfide linkages, and each domain is constructed of two subdomains (IA, IB, etc.). The majority of the compounds are bound at one or both sites within specialized cavities of the subdomains IIA and IIIA with typical equilibrium constants (K) ranging 10^6–10^4 M^{-1} (Kragh-Hansen, 1981a). For instance, bilirubin is primarily bound to a site within IIA. The binding behavior of several porphyrin derivatives to HSA has also been studied over the last two decades (Little et al., 1960; Beaven et al., 1974; Muller-Eberhand et al., 1975; Adams et al., 1980), because hemin released from hemoglobin is transported to the liver by albumin for metabolic processing. The primary binding site of hemin is located in the sequence 124–298 of HSA, corresponding to subdomains Ib–IIa (Hrkal et al., 1984), and the immobilization presumably involves coordination of a histidine residue to the central iron (Casella et al., 1993). The hemopexin in plasma definitely attaches to a free heme in both iron(II) and iron(III) states by an axial imidazole coordination (Muller-Eberhand and Morgan, 1975; Morgan et al., 1980; Lamola et al., 1981). One may expect some new functions of these albumin-heme conjugates, but little attention has been generated so far (Marden et al., 1989; Bonaventura et al., 1994).

We have recently found that a tetraphenylporphyrinatoiron(II) derivative with a covalently linked axial base, 2-[8-{*N*-(2-methylimidazolyl)}octanoyloxymethyl]-5,10,15,20-tetrakis(α,α,α,α-*o*-pivalamido)phenylporphyrinatoiron(II) (FeP, Figure 1) (Tsuchida et al., 1994), is efficiently incorporated into the HSA molecule, providing an artificial hemoprotein which is able to bind and release dioxygen reversibly under physiological conditions (in aqueous media, pH 7.4, 37 °C) as hemoglobin (Komatsu et al., 1995; Tsuchida et al., 1997). The imidazole intramolecularly coordinated to the central iron plays a crucial role in the formation of a stable Fe–O_2 complex. We report herein the stepwise equilibrium constants for FeP association and the physicochemical properties of the obtained hybrid HSA-FeP. Furthermore, the axial base imidazole and the O_2-coordination structures of FeP embedded into certain domains of the albumin have been clarified by resonance Raman spectroscopy.

EXPERIMENTAL PROCEDURES

Materials and Methods. HSA-FeP with different FeP concentration was prepared according to our previously reported procedure (Tsuchida et al., 1997). An HSA was purchased from Bayer Co., Ltd. (Albumin Cutter, 5 wt %). Protoporphyrin IX disodium salts (PPIX) was gifted from Sato Pharmacy Co., Ltd. Phenol red and palmitic

* To whom the correspondence should be addressed. Phone: +81 3-5286-3120; Fax: +81 3-3205-4740. E-mail: eishun@mn.waseda.ac.jp.

† CREST investigator, JST.

10.1021/bc980084p CCC: $18.00
Published on Web 12/31/1998

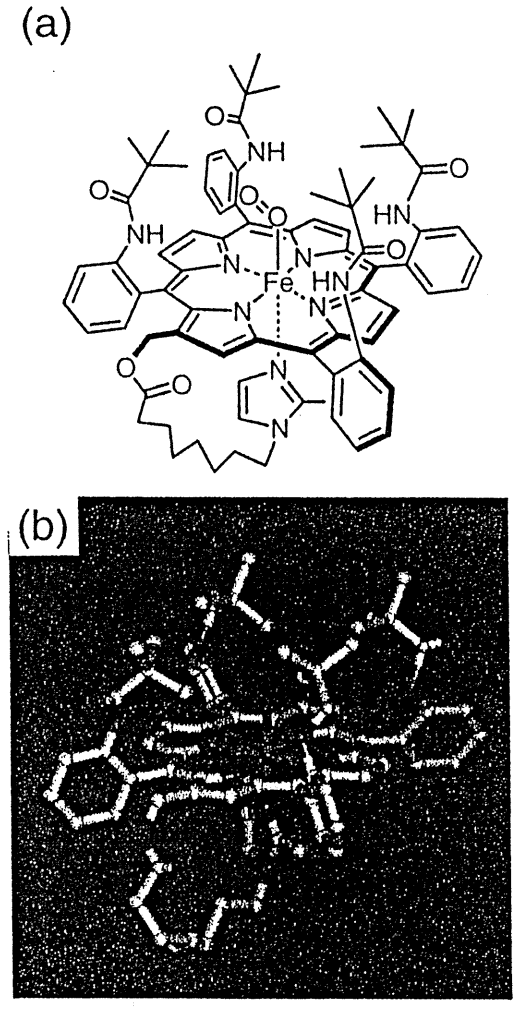

Figure 1. (a) Formula of FeP and (b) computer-simulated structure of dioxygenated FeP. Molecular dynamics and minimization (force field: esff) were performed using an Insight II system (Molecular Simulations Inc.). The structure was generated by alternative minimizations and annealing dynamic calculations from 1000 to 100 K.

acid were purchased from Kanto Chemical Co., Ltd. Pure water (Otsuka Pharmaceutical Co., Ltd.) was used for dilution for HSA and ethanol (>99.5%, Kanto Chemical Co., Ltd.) was for the solvent of FeP. UV–vis absorption spectra were obtained on a Shimadzu V-570 spectrometer.

Equilibrium Constants for FeP Binding to HSA. In the course of preparation of the HSA-FeP solution, the precipitated carbonyl FeP [FeP(CO)] was extracted with $CHCl_3$ and its concentration was determined by the absorption spectra (ϵ_{max} at 420 nm: 2×10^5 $M^{-1}cm^{-1}$). On the basis of the quantitative analysis of this free FeP-(CO) molecule in the solution prepared with different FeP/HSA mixing ratios (1–14 mol/mol), the equilibrium constants were determined using stepwise equilibrium models (Fletcher et al., 1970; Ashbrook et al., 1975).

Binding Sites of FeP in HSA. The association sites of FeP were determined from the competitive binding with other ligands which are well-known to bind the major sites of HSA. Palmitic acid, PPIX, instead of hemin, and phenol red, instead of bilirubin, were used as the inhibitors. The quantitative analysis of FeP was carried out with the hybrid HSA incorporating each inhibitor (molar ratio 1/1). The maximal binding numbers of FeP were decreased to less than the mixing ratio, if the FeP molecule could not displace the inhibitor in competitive binding.

Rheological Properties. The viscosity and density of the solution at 37 °C were measured with an Anton Parr OCR-D oscillatory capillary rheometer and density meter, where the sample in the measuring capillary was set into sinusoidal oscillations at a given frequency of 2 Hz. The shear rate ranged 0.58–358 s^{-1}. The HSA-FeP solution [[HSA]: 5 wt %, FeP/HSA = 4,8 (mol/mol)] was applied to all measurements. The human venous blood were drawn into EDTA containing tube just before use.

Physicochemical Properties. Circular dichroism (CD) spectra were obtained by a JASCO J-725 spectropolarimeter. The HSA concentration was 1.12 μM [FeP/HSA = 1, 4, 8 (mol/mol)], and quartz cuvettes with 1 mm and 10 mm thickness were used for measurements in the ranges 190–250 nm and 250–700 nm, respectively. Isoelectric points and molecular weights were measured by a Pharmacia Phastsystem using isoelectric focusing (IEF) in pH 3–9 Phast Gel IEF 3–9 and native PAGE in Phast Gel Gradient 8–25, respectively. The temperature during the electrophoresis was maintained at 15 °C and the sample concentrations were [HSA] = 3.75 μM. The used markers are Isoelectric Focusing Calibration Kit and LMW Electrophoresis Calibration Kit, respectively. Gel permeation chromatography was performed on a Shimadzu LC-8A chromatograph equipped with a SPD-10A UV–vis detector by using a Shodex GS-620HQ column at room temperature. The HSA-FeP solutions [FeP/HSA = 1, 4, 8 (mol/mol)] were applied to the measurements with phosphate-buffered saline (10 mM, pH 7.3) as the eluent.

Resonance Raman (RR) Spectroscopy. RR spectra were obtained with excitation of the 457.9 nm line of an NEC GLG2162 Ar^+ ion laser in a back-scattering geometry at 25 °C. All the spectra were recorded using a JASCO NRS-2000 laser Raman spectrometer equipped with a CCD multichannel detector. The preparation procedures of the deoxy and dioxygenated HSA-FeP [[HSA]: 5 wt %, FeP/HSA = 4 (mol/mol)] were reported elsewhere (Tsuchida et al., 1997). Calibration of the spectrometer was performed with indene.

RESULTS AND DISCUSSION

Binding Aspects of FeP to HSA. The maximal binding numbers of FeP to one HSA molecule were determined to be eight (Tsuchida et al., 1997). Our second interest in this albumin–heme complex was its nano structure. How strong and at which place are FePs bound in HSA? The binding constants are typically analyzed according to the Scatchard model (Beaven et al., 1974, Halfman and Nishida, 1992), we used, however, another means of analysis with a stepwise equilibrium model (Fletcher et al., 1970; Ashbrook et al., 1975). This model can incorporate many of the concepts in protein–ligand interaction, including cooperativity, the creation of new sites in the binding process, etc.; it is therefore the most satisfactory for protein-heme binding analysis. The magnitude of the binding constants for the FeP association with HSA (K_1–K_8) ranged 1.2×10^6 to 1.3×10^4 M^{-1} (Table 1) in which no cooperative relation was observed. These values are relatively low with respect to those of palmitic acid [K_1–K_8 = (6.2×10^7)–(3.8×10^5) M^{-1}] (Ashbrook et al., 1975) and hemin ($K_1 = 5.0 \times 10^7$ M^{-1}) (Beaven et al., 1974), which have Coulombic interactions with the albumin host through their carboxylic groups. The FeP molecules are probably incorporated into HSA

Table 1. Stepwise Equilibrium Constants of FeP Binding to HSA (M^{-1}) at 25 °C

K_1	K_2	K_3	K_4	K_5	K_6	K_7	K_8
1.2×10^6	7.8×10^4	6.6×10^4	5.3×10^4	2.3×10^4	1.8×10^4	1.7×10^4	1.3×10^4

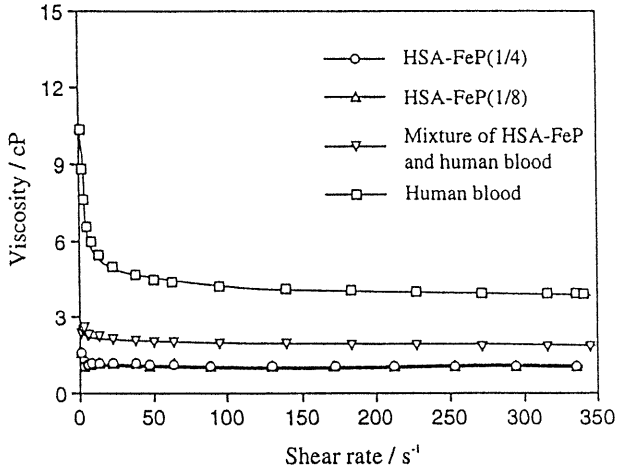

Figure 2. Shear rate dependence of the viscosity of HSA-FeP at 37 °C.

only by hydrophobic interactions, leading to a rather weak nonspecific binding.

The association sites of FeP were estimated from the competitive binding inhibition behavior by other well-known ligands which can bind the typical areas of HSA [palmitic acid (IIIB), PPIX instead of hemin (IB, IIA), and phenol red instead of bilirubin (IIA)]. At an FeP/HSA mixing ratio of 8, the binding numbers were significantly decreased to 7 in all cases; one of the binding regions of the synthetic heme is obviously occupied by the inhibitor ligands. Consequently, the primary binding sites of these ligands are identical to one of the FeP's sites. It is remarkable that the FeP binding was inhibited even by phenol red with a low K_1 of 3.9×10^4 M^{-1} (Kragh-Hansen, 1981b). One of the minor binding sites, at least a fifth one, was definitely blocked by a phenol red molecule.

Structure and Physicochemical Properties. The red-colored solution could be stored for three months at 4 °C; the turbidity at 700 nm was not changed (±4%), and no aggregation was observed for all samples prepared. Furthermore, the solution could be kept as a freeze-dried powder for more than 6 months. The long stability and no blood type, of course, become great advantages of this solution as a dioxygen infusion for potential clinical use.

The solution properties of HSA-FeP sufficiently satisfy the physiological needs. Specific gravities were all 1.013 [FeP/HSA = 1−8 (mol/mol)]. The viscosity behavior showed typical Newtonian type, and a value of 1.1 cP observed at a high shear rate of 230 s^{-1} was much lower than that of human blood (4.0 cP) (Figure 2). Furthermore, the HSA-FeP solution was mixed with fresh drawn human whole blood. The obtained suspension did not show any coagulation or precipitation, and its viscosity behavior was again Newtonian type (1.8 cP at 230 s^{-1}), displaying a good compatibility of HSA-FeP with human blood. The O_2-carrying solution with low viscosity may facilitate circulation and would permit a better exploition of collateral microcirculation.

The physicochemical properties of this artificial hemoprotein were studied. The isoelectric points (pI) of the HSA-FeP [FeP/HSA = 1~8 (mol/mol)] were all found to be 4.8 from the IEF measurements, values that were exactly the same as that of HSA itself (Figure 3a). In the case of fatty acid binding, the pI value significantly decreased due to partial neutralization of the surface charge. Thus, it can be considered that FeP molecules interact nonspecifically with a part (most probably the hydrophobic region) of albumin, and its surface charge distributions are not influenced.

The native PAGE showed the same molecular sizes for all samples with different FeP binding numbers (Figure 3b). This was rather unexpected, because the molecular volume of FeP (1.3^3 nm^3 estimated by simulation, Figure 1b) is relatively bulky as a ligand for the host albumin. The morphology of HSA should be expanded after the FeP incorporation. GPC measurements also displayed very close peaks for HSA and HSA-FeP that could not be clearly distinguished. Carter (1994) reported some preliminary results on cocrystal structures of HSA with long chain fatty acids of laurate or palmitate in which three or more fatty acids bind to produce significant conformational changes in the albumin. The invariable molecular size of HSA-FeP obviously indicates the weak binding of FePs and conformational flexibility of the HSA molecule, somewhat like a sponge.

Circular dichroism (CD) spectroscopy provides information on the secondary and tertiary structures of HSA and conformation changes that ensue when FeP is bound. The spectral pattern showed typical double-minimum negative peaks in the ultraviolet region independent of

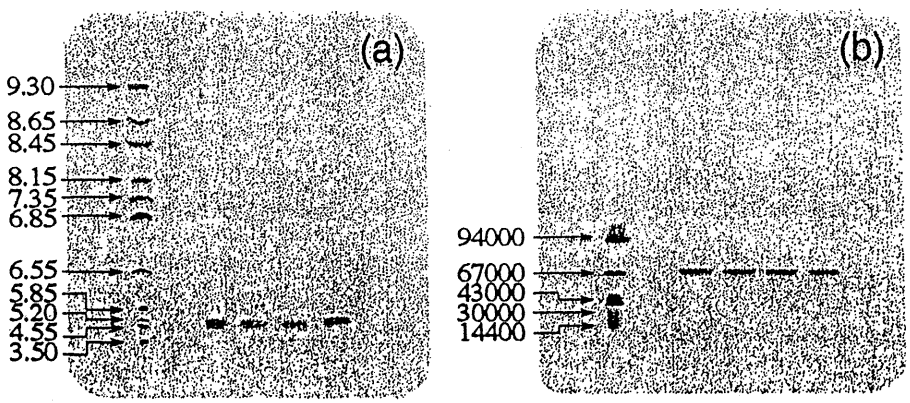

Figure 3. (a) IEF and (b) native-PAGE electrophoretic patterns of HSA and HSA-FeP solution. Lane 1, markers; lane 2, HSA; lane 3, HSA-FeP (1/1); lane 4, HSA-FeP (1/4); lane 5, HSA-FeP (1/8) from the left.

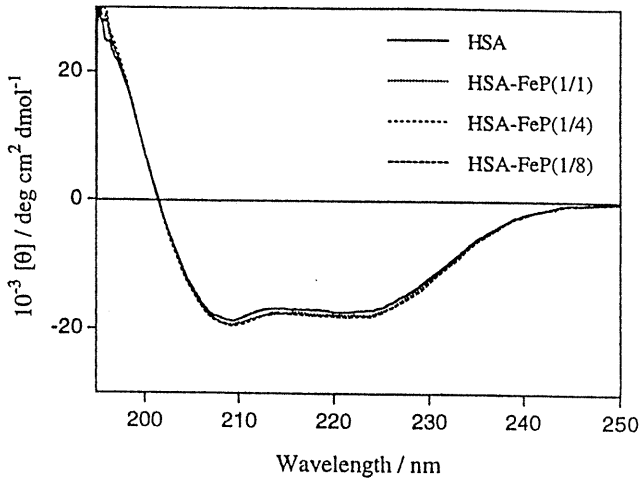

Figure 4. Circular dichroism spectra of the HSA-FeP solution at 25 °C.

the binding numbers of the FeP molecules from one to eight. There are no differences between the HSA-FeP series and HSA itself (Figure 4). The calculated α-helix content was approximately 52%, suggesting that the FeP association did not cause any second- and third-ordered structural changes in HSA. In general, the binding of the heme derivative to the albumin molecule is accompanied by a rise to an extrinsic negative Cotton effect in the Soret band region, because it binds to an albumin through a coordination between the imidazole of histidine and the central iron, allowing a high degree of immobilization (Beaven et al., 1974; Casella et al., 1993). HSA-FeP did not, however, show any CD bands in the Soret region. This observation again indicates a weak interaction between FeP and HSA as an apoprotein.

Attempts to measure the exact molecular mass of HSA-FeP from 67.8 kDa [FeP/HSA = 1 (mol/mol)] to 76.9 kDa [FeP/HSA = 8 (mol/mol)] by a time-of-flight mass spectroscopy with matrix-assisted laser desorption ionization system (Shimadzu Kompact MALDI-4) unfortunately failed. We detected only the 66.5 kDa peak of HSA itself. During the laser ionization, the weakly bound FePs were presumably dissociated from the HSA host. The nonspecific interaction between FeP and HSA was further studied using ultracentrifugation. In all cases, FeP sedimented together with albumin but redispersed again completely on shaking, giving a reddish homogeneous solution which showed the same absorbance at the 420 nm Soret band. We thus concluded that hydrophobic interactions are the major driving force of the FeP binding to HSA and that FeP incorporation does not induce any changes in the highly ordered structure and surface charge distribution of the albumin molecule.

Resonance Raman Studies of Axial Ligand Coordination to FeP Incorporated into HSA. The obtained HSA-FeP has the ability to bind dioxygen reversibly at 37 °C with a constant O_2-binding affinity [$P_{1/2}(O_2)$: 30 Torr], independent of the numbers of associated FePs (Tsuchida et al., 1997). The auto-oxidation reaction of the oxy state (λ_{max}: 548 nm) took place slowly, and the absorption band of 548 nm almost disappeared after 24 h, leading to formation of inactive hemin. The half-life ($\tau_{1/2}$) of the dioxygenated species was 8 h at 25 °C. We employed resonance Raman (RR) spectroscopy to characterize the O_2-coordination structure of the dioxygenated FeP in HSA. Soret band excitation of natural hemoproteins or synthetic porphyrinatoiron(II)s resulted in rich RR spectra consisting of totally symmetric vibrations of

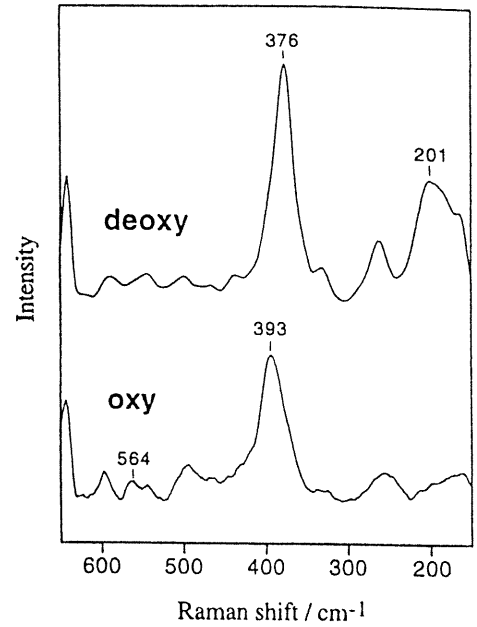

Figure 5. Resonance Raman spectra of the HSA-FeP solution at 25 °C.

the porphyrin macrocycle (Spiro et al., 1975). In the low-frequency RR spectra (<650 cm^{-1}) of the HSA-FeP under argon (i.e., the deoxy form), there is a medium band at 201 cm^{-1} (Figure 5). The five-coordinated species of FeP in CH_2Cl_2 also displayed a similar band at 205 cm^{-1} that has been assigned to the intramolecular coordinated iron–imidazole stretching mode, ν(Fe–N_ϵ) (Wu et al., 1998). The covalently attached imidazole allowed the intramolecular iron–imidazole coordination of FeP even when embedded into a hydrophobic binding domain of the protein, where other peptide residues possibly coordinated to the central iron(II) may exist.

In addition, several porphyrin skeletal modes, that are sensitive to the spin state, have been identified (Burke et al., 1978). For instance, a relatively strong band around 360–395 cm^{-1} for tetraphenylporphyrinatoiron(II) derivatives has been assigned to a deformation mode of the porphyrin ring (ν_8) (Stein et al., 1984). The appearance of a ν_8 band at 376 cm^{-1} for HSA-FeP under argon represented the formation of the high-spin five-coordination state (Figure 5). Other strong bands at 1340–1390 cm^{-1} are generally assigned to a ν_4 frequency, a deformed pyrrole-ring breath-like mode (Oshio et al., 1984; Proniewicz et al., 1986), that depends on the electron density at the π^* antibonding orbital of the porphyrin (Abe et al., 1978). Hence, it is sensitive to the axial coordination state of the central iron. The ν_4 band of the deoxy HSA-FeP at 1356 cm^{-1} corresponding to the five-coordinated high-spin species immediately shifted to 1371 cm^{-1} after exposure to dioxygen. This observation indicated the formation of a six-coordinated low-spin dioxygenated species. At the same time, in the low-frequency region, the ν(Fe–O_2) vibration appeared at 564 cm^{-1}. This frequency mode represented the formation of dioxygenated heme with an end-on type coordinated dioxygen, similar to hemoglobin and myoglobin. All these peak changes have been observed to be reversibly dependent on the O_2 concentration. We concluded that the FePs having an intramolecular coordinated imidazole group obviously bind and release dioxygen in the HSA molecule.

In conclusion, human serum albumin incorporating synthetic hemes as O_2-binding sites provides an O_2

carrying artificial hemoprotein as a hemoglobin analogue and shows unique physicochemical properties. The heme binding through hydrophobic interaction is relatively weak and does not lead to a change in the morphology and highly ordered structure, as well as the solution properties of HSA, independent of the binding numbers of FeP. The imidazole moiety coordinates to the central iron producing a five-coordinated high-spin species, and the complex forms a reversible and stable dioxygen adduct in HSA. Evaluation of the O_2-delivering efficacy in vivo is now underway using hemorrhagic shocked rats. HSA-FeP acts as a new O_2-carrying hemoprotein molecule capable of replacing hemoglobin in the bloodstream.

There is also current interest in recombinant HSA (rHSA), which has been recently manufactured by gene cloning and expression in *Pichia pastoris* (Sumi et al., 1993). A study on an rHSA–FeP conjugate as a totally synthetic O_2-carrier is also in progress.

ACKNOWLEDGMENT

This work was partially supported by the Health Science Research Grants (Artificial Blood Project), the Ministry of Health and Welfare, Japan.

LITERATURE CITED

Abe, M., Kitagawa, T., and Kyogoku, Y. (1978) Resonance Raman Spectra of Octaethylporphyrinato-Ni(II) and Meso-Deuterated and ^{15}N Substituted Derivatives. II. A Nomal Coordinate Analysis. *J. Chem. Phys. 69,* 4526–4534.

Adams, P. A., and Berman, M. C. (1980) Kinetics and Mechanism of the Interaction Between Human Serum Albumin and Monomeric Haemin, *Biochem. J. 191,* 95–102 (1980).

Ashbrook, J. D., Sector, A. A., Santos, E. C., and Fletcher, E. (1975) Long Chain Fatty Acid Binding to Human Plasma Albumin. *J. Biol. Chem. 250,* 2333–2338.

Beaven, G. H., Chen, S.-H., D'Albis, A., and Gratzer, W. B. A Spectroscopic Study of the Haemin-Human-Serum-Albumin System. (1974) *Eur. J. Biochem. 41,* 539–546.

Bonaventura, J., Brouwer, M., Brouwer, T., Cashon, B., and Cameron, S. (July 1994) Presented in part at the 11th Congress ISABI, Boston.

Brown, J. R. (1976) Serum Albumin: Amino Acid Sequence. in *Albumin Structure, Function and Uses* (V. M. Rosenoer, M. Oratz, and M. A. Rothschild, Eds.) pp 27–51 Pergamon Press, New York.

Burke, J. M., Kincaid, J. R., Peters, S., Gagne, R. R., Collman, J. P., and Spiro, T. G. (1978) Structure-Sensitive Resonance Raman Bands of Tetraphenyl and "Picket Fence" Porphyrin-Iron Complexes, Including an Oxyhemoglobin Analogue. *J. Am. Chem. Soc. 100,* 6083–6088.

Carter, D. C., and Ho, J. X. (1994) Structure of Serum Albumin. *Adv. Protein Chem. 45,* 153–203.

Carter, D. C., He, X.-M., Munson, S. H., Twigg, P. D., Gernert, K. M., Broom, M. B., and Miller, T. Y. (1989) Three-Dimensional Structure of Human Serum Albumin. *Science 244,* 1195–1198.

Casella, L., Gullotti, M., Poli, S., and De Gioia, L. (1993) Haem-Protein Interactions. The Binding of Haem Complexes to Serum Albumin. *Gazz. Chim. Ital. 123,* 149–154.

Fletcher, J. E., Sector, A. A., and Ashbrook, J. D. (1970) Analysis of Macromolecule-Ligand Binding by Determination of Stepwise Equilibrium Constants. *Biochemistry 9,* 4580–4587.

Halfman, C. J., and Nishida, T. (1972) Method for Measuring the Binding of Small Molecules to Proteins from Binding-Induced Alterations of Physical Chemical Properties. *Biochemistry 11,* 3493–3498.

He, X. M., and Carter, D. C. (1992) Atomic Structure and Chemistry of Human Serum Albumin. *Nature 356,* 209–215.

Hrkal, Z., and Klementova, S. (1984) Bilirubin and Haem Binding to Human Serum Albumin Studied by Spectroscopy Methods. *J. Biochem. 16,* 799–804.

Komatsu, T., Ando, K., Kawai, N., Nishide, H., and Tsuchida, E. (1995) O_2-Transport Albumin: A New Hybrid-Haemoprotein Incorporating Tetraphenylporphyrinato-iron(II) Derivative. *Chem. Lett. 1995,* 813–814.

Kragh-Hansen, U. (1981a) Molecular Aspects of Ligand Binding to Serum Albumin. *Pharmacol. Rev. 33,* 17–53.

Kragh-Hansen, U. (1981b) Effect of Aliphatic fatty Acids on the Binding of Phenol Red to Human Serum Albumin. *Biochem. J. 195,* 603–613.

Lamola, A. A., Asher, I., Muller-Eberhard, U., and Poh-Fitzpatrick, M. (1981) Fluorimetric Study of Binding of Protoporphyrin to Haemopexin and Albumin. *Biochem. J. 196,* 693–698.

Little, H. N., and Nelands, J. B. (1960) Binding of Hematin by Human Serum Albumin. *Nature 170,* 913–915.

Marden, M. C., Hazard, E. S., Leclerc, L., and Gibson, Q. H. (1989) Flash Photolysis of the Serum Albumin–Heme-CO Complex. *Biochemistry 28,* 4422–4426.

Morgan, W. T., Smith, A., and Koskelo, P. (1980) The Interaction of Human Serum Albumin and Hemopexin with Porphyrins. *Biochim. Biophys. Acta 624,* 271–285.

Muller-Eberhand, U. and Morgan, W. T. (1975) Porphyrin-Binding Proteins in Plasma. *Ann. N.Y. Acad. Sci. 244,* 625–650.

Oshio, H., Ama, T., Watanabe, T., Kincaid, J., and Nakamoto, K. (1984) Structure Sensitive Bands in the Vibrational Spectra of Metal Complexes of Tetraphenyl-porphine. *Spectrochim. Acta 40A,* 863–870.

Peters, T., Jr. (1975) Serum Albumin. *The Plasma Proteins. Structure, Function and Genetic Control* (F. W. Putnum, Ed.) 2nd ed., pp 133–181, Academic Press, New York.

Peters, T., Jr. (1985) Serum Albumin. *Adv. Protein Chem. 37,* 161–245.

Proniewicz, L. M., Bajdor, K., and Nakamoto, K. (1986) Resonance Raman Spectra of Ferrylporphyrins and Related Compounds in Dioxygen Matrixes. *J. Phys. Chem. 90,* 1760–1766.

Spiro, T. G. (1975) Resonance Raman Spectroscopic Studies of Heme Proteins. *Biochim. Biophys. Acta 416,* 169–187.

Stein, P., Ulman, A., and Spiro, T. G. (1984) Resonance Raman Spectra of S_2TPP, SSeTPP, Se_2TPP and H_2TPP: Extended Tetraphenylporphine Vibrational Assignments and Bonding Effects. *J. Phys. Chem. 88,* 369–374.

Sumi A, Ohtani, W., Kobayashi, K., Ohmura, T., Yokoyama, K., Nishida, M., and Suyama, T. (1993) Purification and Physicochemical Properties of Recombinant Human Serum Albumin. in *Biotechnology of Blood Proteins* (J. Rivat, and J. F. Stolts, Eds.) Vol. 227, pp 293–298, John Libbey Eurotext.

Tsuchida, E., Komatsu, T., Kumamoto, S., Ando, K., and Nishide, H. (1994) Synthesis and O_2–Binding Properties of Tetraphenylporphyrinatoiron(II) Derivatives Bearing a Proximal Imidazole Covalently Bound at the β-pyrrolic Position. *J. Chem. Soc., Perkin Trans. 2 1995,* 747–753.

Tsuchida, E., Ando, K., Maejima, H., Kawai, N., Komatsu, T., Tekeoka, S., and Nishide, H. (1997) Properties of and Oxygen Binding by Albumin-Tetraphenyl-porphinatoiron(II) Derivative Complexes. *Bioconjugate Chem. 8,* 534–538.

Wu, J., Komatsu, T., Tsuchida, E. (1998) Resonance Raman Studies of O_2–Binding to *ortho*-Substituted Tetraphenyl- and Tetranaphthyl-Porphyrinatoiron(II) Derivatives with a Covalently Linked Axial Imidazole. *J. Chem. Soc., Dalton Trans. 1998,* 2503–2506.

BC980084P

ART. CELLS, BLOOD SUBS., AND IMMOB. BIOTECH., 26(5&6), 487-495 (1998)

EFFECTS OF LIPOSOME-ENCAPSULATED HEMOGLOBIN ON PHORBOL ESTER-INDUCED SUPEROXIDE PRODUCTION AND EXPRESSION OF COSTIMULATORY MOLECULES BY MONOCYTES IN VITRO

M. Fujihara, K. Ikebuchi, M. Yamaguchi, H. Abe,
K. Niwa, and S. Sekiguchi.
Hokkaido Red Cross Blood Center, Sapporo 063, Japan

ABSTRACT

The effects of Neo Red Cell (NRC), a liposome-encapsulated hemoglobin (LEH), on the phorbol ester-induced superoxide production and the expression of costimulatory molecules by human peripheral monocytes were investigated. The treatment of human mononuclear cells with NRC caused the potentiation of superoxide production in response to PMA. The longer incubation (20 h) resulted in a decrease in the PMA-induced superoxide production, which was in parallel to a decrease in the viability of the monocytes. A flow cytometric analysis showed that a slight expression of CD80 (B7-1) on monocytes was induced by NRC treatment, whereas the constitutive expressions of CD86 (B7-2) and CD54 (ICAM-1) were unchanged. The activation of monocytes with interferon-γ (IFN-γ) induced the expressions of CD80, CD86, and CD54 under all conditions tested, but NRC treatment tended to decrease the IFN-γ-induced expression of CD54 on monocytes. These results suggest that the administration of LEH may modify the functions of human monocytes.

INTRODUCTION

Liposome-encapsulated hemoglobin (LEH) has been developed as a red blood cell substitute, and the efficacy of this material has been demonstrated in total isovolemic exchange transfusions, hemorrhagic shock and hemodilution states in animal models (1-5). Because the reticuloendothelial systems as well as the lungs are largely responsible for the removal of LEH from the circulation, the effects of LEH on the immunoresponse of fixed tissue macrophages have been well studied (6-8). A biodistribution study using radio-labeled LEH

showed a significant retention of LEH (~50%) in the blood at 20 h after administration (9). Hence, LEH administration may affect the functions of human monocytes during retention in the circulation.

In this study, we investigated the functional interactions between LEH and human peripheral monocytes, focussing on the phorbol ester-induced superoxide production and expression of costimulatory molecules by these monocytes, which play important roles in immune responses.

MATERIALS AND METHODS

Treatment of mononuclear cells with NRC or empty liposomes

Peripheral blood mononuclear cells (PBMCs) were prepared from peripheral blood by Ficoll/Paque density sedimentation and cultured in RPMI-1640 containing 10% human AB serum, 100 U/ml penicillin, and 100 μg/ml streptomycin. The LEH used was Neo Red Cell (NRC; Terumo Inc., Tokyo, Japan). NRC is human stroma-free hemoglobin encapsulated in lipid vesicles. Lipids are composed of a 7:7:2:0.28 ratio of soybean hydrogenated phosphatidylcholine, cholesterol, myristic acid, α-tocopherol. The size of NRC is approximately 250 nm in diameter. Empty liposomes (Liposome) have the same lipid composition as NRC, but their size is approximately half that of NRC. Superficial modification of both NRC and empty liposomes was carried out by the use of polyethyleneglycol-conjugated phosphatidylethanolamine and for preventing agglutination. The PBMCs were treated with NRC or empty liposomes at the concentrations indicated in each figure. Interferon (IFN)-γ (Boehringer Mannheim, Mannheim, Germany) was used at a final concentration of 500 U/ml.

Superoxide production assay

Superoxide (O_2^-) production was detected by a chemiluminescence method. NRC- or liposome-treated PBMCs (~ 2 x 10^7 cells) were washed with Hank's balanced salt solution (HBSS). The cells were preincubated at 37°C, and incubated with 50 μM cypridina luciferin analog (Tokyo Kasei, Tokyo, Japan). After the addition of phorbol myristate acetate (PMA) at a final concentration of 1 μM, the chemiluminescence was measured with a chemiluminescence reader (Biolumat LB 9500 C: Berthold Japan, Japan).

Flow cytometric analysis

PBMCs were treated with NRC or empty liposomes for 20 hr. The nonadherent cells were harvested, and the adherent cells were detached by incubation with 1 mM EDTA/phosphate-buffered saline (PBS) for 30 min at 4°C. The collected cells were washed with PBS, and stained with propidium iodide (PI), fluorescein isothiocyanate (FITC)-conjugated anti-CD14 MoAb (Immunotech, Marseille Cedex, France), anti-CD54 MoAb (Immunotech),

phycoerythrin (PE)-conjugated anti-CD80 MoAb (Becton Dickinson, San Jose, CA, USA) and anti-CD86 MoAb (PharMingen, San Diego, CA, USA). Two-color immunofluorescence analysis was performed on an ORTHO CYTORON system (Ortho Diagnostic Systems Inc., Raritan, NJ, USA).

RESULTS

Effects of NRC and Liposome treatment on PMA-induced O_2^- production in mononuclear cells

We first studied the effect of NRC or empty liposomes on superoxide production by PBMCs using PMA as a stimulus. The PBMCs were treated with various concentrations of NRC or liposome for up to 150 min. As shown in Fig.1, the treatment of PBMCs with NRC (5%) caused a considerable increase in PMA-induced superoxide production. The treatment of cells with empty liposomes also resulted in a dose-dependent enhancement. The effect of the liposomes was more evident than that of NRC.

Next, we studied the effect of a longer incubation (20 hr) with NRC or liposomes on the PMA-induced superoxide production. Figure 2 shows that the treatment of PBMCs with NRC caused a dose-dependent decrease in the superoxide production. The same effect was observed in the case of empty liposomes. The concomitant treatment of IFN-γ, a potent activator for monocytes, appeared to cause a further reduction.

Analysis of cell viability by flow cytometry

To test the possibility that the reduction of superoxide production is due to the toxicity of NRC, cell viability was assessed by flow cytometry using PI staining. PI-positive cells are recognized as dead cells. Figure 3 shows that the side scatter of the monocytes was increased as the concentration of NRC increased, while the side scatter of lymphocytes was unchanged. This result suggests that NRC was taken up by monocytes, causing the changes of intracellular structure. Furthermore, the forward scatter of monocytes was reduced with the increasing concentrations of NRC, indicating that the NRC treatment caused the reduction of monocyte size. There was no effect on lymphocytes. Figures 4 and 5 showed that the NRC treatment caused a dose-dependent cell death of monocytes. Incubation with NRC at 5% caused a more than 90% reduction of monocyte viability. This reduction of cell viability was specific for monocytes, since lymphocytes were not stained with PI (data not shown). Thus, the reduction of monocyte viability by NRC treament was in parallel with the decrease of PMA-induced superoxide production, suggesting that the reduction of PMA-induced superoxide production by NRC treatment for 20 hr is mainly attributed to the decrease in cell viability of monocytes.

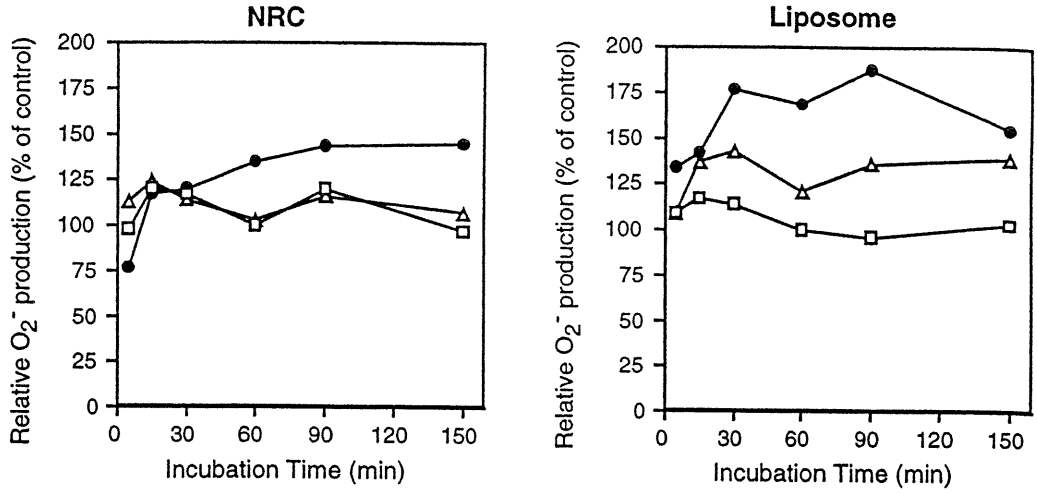

Figure 1: Effects of NRC and empty liposomes on the PMA-induced superoxide production by PBMCs. PMA-induced superoxide production by PBMCs without NRC or liposomes was used as a control. Representative data from three independent experiments are shown. (□) 1%, (≥) 2.5%, (●) 5%.

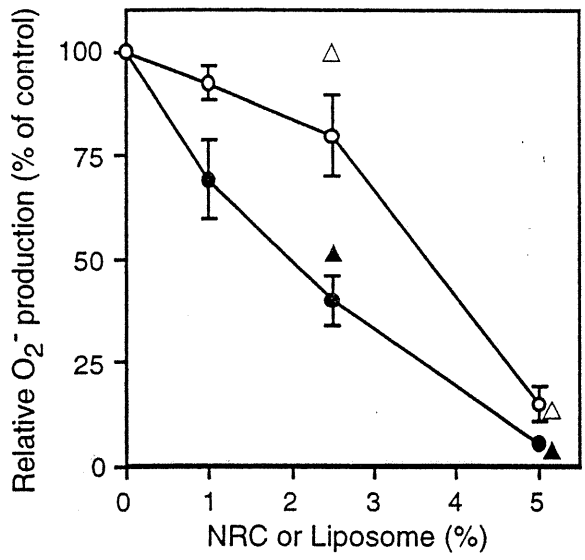

Figure 2: Effects of NRC (circles) and empty liposomes (triangles) on PMA-induced superoxide production (20 hr after treatment). PBMCs were treated for 20 hr with NRC at the concentrations indicated plus (closed) or minus (open) IFN-γ. PMA-induced superoxide production by cells without NRC or liposomes was used as a control. The values are the mean ± SE from three donors.